[American Journal of Science, Vol. 310, April, 2010, P. 282–324, DOI 10.2475/04.2010.03]

EVALUATION OF TRAPPING MECHANISMS IN GEOLOGIC CO_2 SEQUESTRATION: CASE STUDY OF SACROC NORTHERN PLATFORM, A 35-YEAR CO_2 INJECTION SITE

WEON SHIK HAN*†, BRIAN J. MCPHERSON**, PETER C. LICHTNER***, and FRED P. WANG§

ABSTRACT. **CO_2 trapping mechanisms in geologic sequestration are the specific processes that hold CO_2 underground in porous formations after it is injected. The main trapping mechanisms of interest include (1) fundamental confinement of mobile CO_2 phase under low-permeability caprocks, or stratigraphic trapping, (2) conversion of CO_2 to mineral precipitates, or mineral trapping, (3) dissolution in *in situ* fluid, or solubility trapping, and (4) trapping by surface tension (capillary force) and, correspondingly, remaining in porous media as an immobile CO_2 phase, or residual CO_2 trapping. The purpose of this work is to evaluate and quantify the competing roles of these different trapping mechanisms, including the relative amounts of storage by each. For the sake of providing a realistic appraisal, we conducted our analyses on a case study site, the SACROC Unit in the Permian basin of western Texas. CO_2 has been injected in the subsurface at the SACROC Unit for more than 35 years for the purpose of enhanced oil recovery. Our analysis of the SACROC production and injection history data suggests that about 93 million metric tons of CO_2 were injected and about 38 million metric tons were produced from 1972 to 2005. As a result, a simple mass-balance suggests that the SACROC Unit has accumulated approximately 55 million metric tons of CO_2.**

Our study specifically focuses on the northern platform area of the SACROC Unit where about 7 million metric tons of CO_2 is stored. In the model describing the SACROC northern platform, porosity distributions were defined from extensive analyses of both 3-D seismic surveys and calibrated well logging data from 368 locations. Permeability distributions were estimated from determined porosity fields using a rock-fabric classification approach. The developed 3-D geocellular model representing the SACROC northern platform consists of over 9.4 million elements that characterize detailed 3-D heterogeneous reservoir geology. To facilitate simulation using conventional personal computers, we upscaled the 9.4 million elements model using a "renormalization" technique to reduce it to 15,470 elements. Analysis of groundwater chemistry from both the oil production formations (Cisco and Canyon Groups) and the formation above the sealing caprock suggests that the Wolfcamp Shale Formation performs well as a caprock at the SACROC Unit. However, results of geochemical mixing models also suggest that a small amount of shallow groundwater may be contaminated by reservoir brine possibly due to: (1) downward recharge of recycled reservoir brine from brine pits at the surface, or (2) upward leakage of CO_2-saturated reservoir brine through the Wolfcamp Shale Formation.

Using the upscaled 3-D geocellular model with detailed fluid injection/production history data and a vast amount of field data, we developed two separate models to evaluate competing CO_2 trapping mechanisms at the SACROC northern platform. The first model simulated CO_2 trapping mechanisms in a reservoir saturated with brine only. The second model simulated CO_2 trapping mechanisms in a reservoir saturated with both brine and oil. CO_2 trapping mechanisms in the brine-only model show distinctive stages accompanying injection and post-injection periods. In the 30-year

* Energy and Geoscience Institute, University of Utah, Salt Lake City, Utah 84108 USA
** Department of Civil and Environmental Engineering, University of Utah, Salt Lake City, Utah 84112 USA
*** Subsurface Flow and Transport, EES-16, MS D469, Los Alamos National Laboratory, Los Alamos, New Mexico 87575, USA
§ Texas Bureau of Economic Geology, Austin, Texas 78713-8924
† Corresponding author: Weon Shik Han (wshan@egi.utah.edu)

injection period from 1972 to 2002, the amount of mobile CO_2 increased to 5.0 million metric tons without increasing immobile CO_2, and the mass of solubility-trapped CO_2 sharply rose to 1.7 million metric tons. After CO_2 injection ceased, the amount of mobile CO_2 dramatically decreased and the amount of immobile CO_2 increased. Relatively small amounts of mineral precipitation (less than 0.2 million metric tons of CO_2 equivalent) occurred after 200 years. In the brine-plus-oil model, dissolution of CO_2 in oil (oil-solubility trapping) and mobile CO_2 dominated during the entire simulation period. While supercritical-phase CO_2 is mobile near the injection wells due to the high CO_2 saturation, it behaves like residually trapped CO_2 because of the small density contrast between oil and CO_2. In summary, the brine-only model reflected dominance by residual CO_2 trapping over the long term, while CO_2 in the brine-plus-oil model was dominated by oil-solubility trapping.

Key words: Carbon dioxide, Geologic sequestration, CO_2 trapping mechanisms, Heterogeneity, Numerical Simulation, SACROC Unit.

INTRODUCTION

Over the past decade, the international scientific and engineering communities investigated the feasibility of long-term geologic sequestration of CO_2 in deep saline formations as a means of reducing atmospheric CO_2 levels (IEA, 2001; Gale, 2004; Orr, 2004; Thomas and Benson, 2005; Holloway, 2005; IPCC, 2005). Fundamental science questions considered and evaluated previously include:

1. **The physico-chemical properties of CO_2, brine, and CO_2-brine for predicting multiphase transport and solubility trapping** (Spycher and others, 2003; Duan and Sun, 2003; Bando and others, 2004; Portier and Rochelle, 2005; Spycher and Pruess, 2005; Dubessy and others, 2005; Duan and others, 2006, 2008; Fuller and others, 2006; Hu and others, 2007; Fleury and Deschamps, 2008; McPherson and others, 2008),
2. **Storage capacity estimation including appropriate storage site selection** (Bachu and Adams, 2003; NETL, 2005; Bradshaw and others, 2007; Bachu and others, 2007; Dilmore and others, 2008; Litynski and others, 2008; Núñez-López and others, 2008; Kopp and others, 2009),
3. **Spatiotemporal trapping mechanisms including hydrodynamic, residual, solubility, and mineral trappings** (Ennis-King and Paterson, 2005, 2007; Doughty and Pruess, 2004; Xu and others, 2004, 2005; Hellevang and others, 2005; Knauss and others, 2005; White and others, 2005; van der Meer and van Wees, 2006; Zerai and others, 2006; Farajzadeh and others, 2007; Ide and others, 2007; Parry and others, 2007; Flett and others, 2007; Audigane and others, 2007; Suekane and others, 2008; Zhou and others, 2008; Qi and others, 2009; Zhang and others, 2009),
4. **Caprock integrity** (Gaus and others, 2005; Chiquet and others, 2007; Gherardi and others, 2007; Plug and Bruining, 2007; Busch and others, 2008; Lu and others, 2009),
5. **Monitoring and verification including plume migration and groundwater impact** (Klusman, 2003; Emberley and others, 2004; Lewicki and others, 2005; Winthaegen and others, 2005; Gasperikova and Hoversten, 2006; Saripalli and others, 2006; Wells and others, 2007; Newell and others, 2008),
6. **Potential of CO_2 release from geologic storage sites** (Altevogt and Celia, 2004; Nordbotten and others, 2005; Pruess, 2005, 2008; Barlet-Gouêdard and others, 2006; Oldenburg and Lewicki, 2006; Watson and Bachu, 2007; Cortis and others, 2008).

While these studies have successfully addressed most aspects of these questions, effective prediction of spatiotemporal CO_2 trapping mechanisms (mobile CO_2, residual CO_2, dissolved CO_2, and mineral) is still a challenging problem because it is

greatly affected by variability of subsurface conditions (pressure, temperature, and salinity), fluid properties (density, viscosity, solubility), and rock properties (porosity, permeability, and geochemical reactivity of minerals). Doughty and Pruess (2004) attempted to predict solubility trapping using a three-dimensional heterogeneous model of the fluvial/deltaic Frio Formation. They performed a numerical simulation to estimate CO_2 solubility trapping and storage capacity. Although their results showed strong interplay between geological heterogeneity and buoyancy-driven CO_2 flow, their model neglected both residual and mineral trapping. Kumar and others (2005) simulated the temporal variation of CO_2 trapping mechanisms in generalized three-dimensional, log-normally distributed permeability fields. They concluded that the relative degree of residual CO_2 trapping could be significantly greater than both solubility and mineral trapping mechanisms. Since residual CO_2 trapping is regarded as a most-effective trapping mechanism during the short term (hundreds of years), several studies specifically focused on investigating various aspects (for example, hysteresis, injection rate, water-alternating gas, and heterogeneity) to improve residual CO_2 trapping (Juanes and others, 2006; Ide and others, 2007; Flett and others, 2007; Doughty, 2007; Qi and others, 2009; Han and others, 2010a). Likewise, studies of mineral trapping include Xu and others (2004, 2005), Gaus and others (2005), White and others (2005), Zerai and others (2006), Audigane and others (2007), and Zhang and others (2009). Several different simulators were used in these studies, including TOUGHREACT, EQ3/6, CMG's GEM-GHG, ChemTOUGH2, PHREEQC, and Geochemist's Workbench (Wolery and Daveler, 1992; White, 1995; Bethke, 1996; Parkhurst and Appelo, 1999; Nghiem and others, 2004; Xu and others, 2006).

Despite the great deal of research on CO_2 trapping mechanisms, previous attempts to predict CO_2 trapping mechanisms appear to be hampered by several limitations:

(1) Most previous models did not explicitly couple all CO_2 trapping mechanisms simultaneously. Rather, model simulations were focused on predicting one or two specific mechanisms.
(2) Most previous models simplified their dimensions into either one or two, and neglected effects of heterogeneity.
(3) Although some of the models used a three-dimensional grid, either spatial heterogeneity or the CO_2 injection data measured from the field were disregarded or not available.

A primary purpose of this research was to provide a detailed analysis of spatiotemporal CO_2 trapping mechanisms. We focused our analysis on a case study of the Scurry Area Canyon Reef Operations Committee (SACROC) Unit, a site with an abundance of actual CO_2 injection and production data; over 93 million metric tons of CO_2 were injected for the purpose of enhanced oil recovery since 1972 (Raines and others, 2001). We selected this site because vast amounts of data are available including (1) fluid injection/production history data since 1948, (2) water chemistry data of both reservoir brine and shallow groundwater, and (3) a 3-D high-resolution geocellular model that includes detailed characterization of reservoir structure and heterogeneity. The 3-D geocellular model employed in this study was developed using high-resolution geologic data (core data, well-logging data, sedimentologic and stratigraphic interpretation) and geophysical data (seismic attributes and rock physics data).

CO_2 Injection Site: SACROC Unit, Texas

Geologic Descriptions

The SACROC Unit is located in the southeastern segment of the Horseshoe Atoll within the Midland basin, western Texas (figs. 1A and B). Within the Horseshoe Atoll, the SACROC Unit comprises an area of 356 km^2 with an approximate north-south

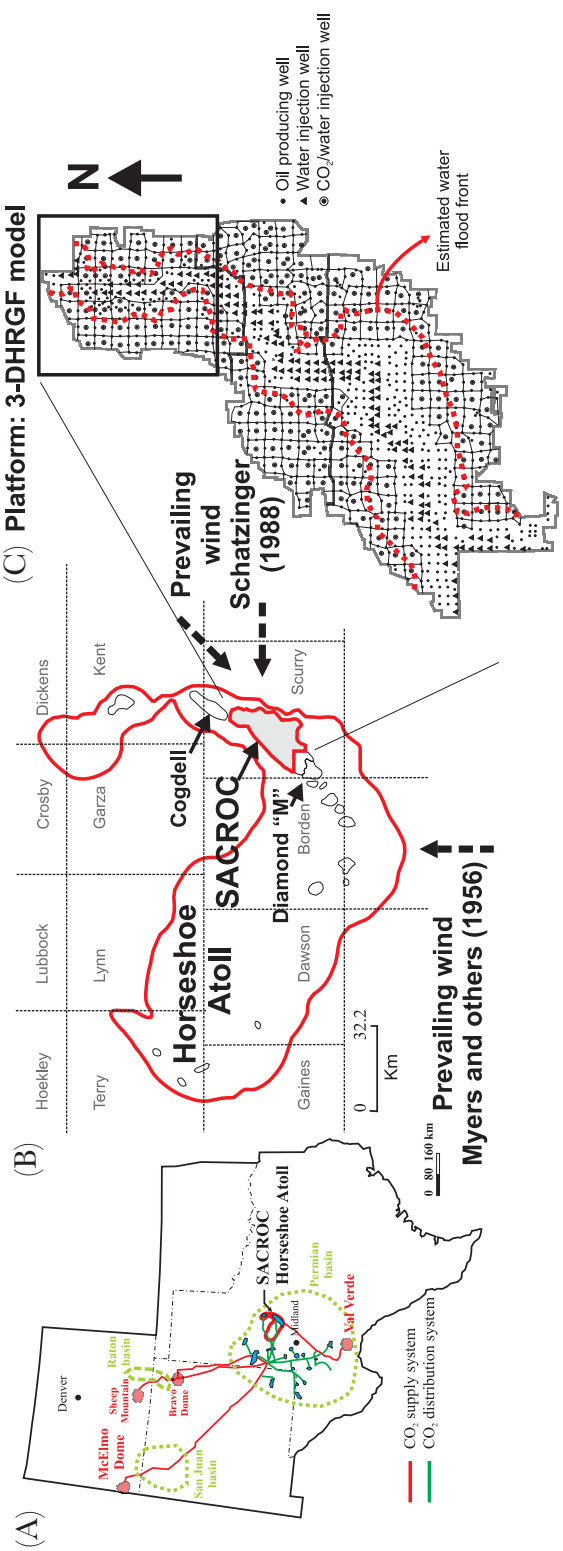

Fig. 1. (A) SACROC Unit at the Horseshoe Atoll in western Texas and CO_2 supply system from natural CO_2 reservoirs, (B) Magnified map of the SACROC Unit within the Horseshow Atoll with indication of paleo-wind direction, (C) Well locations of SACROC Unit with the estimated water-flooding fronts at the end of water-flooding period in 1973 (Kane, 1979).

length of 40 km and an east-west length of 3 to 15 km (Vest, 1970). Geologically, the SACROC Unit is composed of massive amounts of bedded bioclastic limestone and thin shale beds representing the Strawn, Canyon, and Cisco Groups of the Pennsylvanian (Vest, 1970; Raines and others, 2001). The Wolfcamp Shale Formation of the lower Permian provides a low permeability caprock above the Pennsylvanian Cisco and Canyon Groups in the SACROC Unit. In detail, the Cisco and Canyon Groups are mostly composed of limestone with minor amounts of anhydrite. Sand, chert, and shale are present locally. Recently, Carey and others (2007) analyzed core samples from wells 49-5 and 49-6 in the SACROC Unit and indicated that the limestone was mostly calcite with minor ankerite, quartz, and thin clay lenses.

Previously, many petroleum geologists studied the SACROC Unit with respect to facies, depositional environment, and petrography (Bergenback and Terriere, 1953; Myers and others, 1956; Stafford, 1957; Stewart, ms, 1957; Burnside, 1959; Vest, 1970; Schatzinger, 1988; Reid and Reid, 1991; Walker and others, 1991; Raines and others, 2001). Several investigators have attempted to identify the depositional environments from the present distribution of carbonate lithofacies in this area. Their goal was to deduce the spatial locations of the high porosity zones to improve oil production by understating the depositional environment. Initially, Bergenback and Terriere (1953) inferred depositional environments from the distribution of carbonate lithofacies such as calcilutite (calcite mud) and oolitic limestone, which were respectively deposited in environments with calm water and strong currents. Myers and others (1956) discussed the possible theories of atoll growth and concluded that the "winds and currents" theory by Fairbridge (1950) accounted for the shape of the Horseshoe Atoll. Their research deduces conclusions that the direction of prevailing wind and currents was from south to north (fig. 1B). Later, Schatzinger (1988) recognized the spatial variation of oolites, which evidently decrease from north (Cogdell field) to south (Diamond M field), in the eastern portions of the Horseshoe Atoll and inferred that sedimentation was influenced by east-northeast prevailing winds (fig. 1B). Walker and others (1991) tried to identify the distribution of carbonate species and accretion of the Horseshoe Atoll by placing it in its paleolatitude and paleogeographic orientation (fig. 2). According to their research, the carbonate platform was on the equator in the early Strawn (312 Ma). From early Strawn (312 Ma) to middle Canyon (306 Ma), the relative motion of the carbonate platform was 63 degrees northeast and the platform accumulated at 2 degrees north. From early Cisco (298 Ma) to Wolfcampian (280 Ma), the direction of movement changed to 24 degrees northeast. As a result, the platform moved from 2 to 4 degrees north. Finally, carbonate accumulation stopped during the Wolfcampian at 6 degrees north due to the influx of fine-grained siliciclastics and dark shales (Walker and others, 1991). During its accumulation, prevailing winds from the northeast had a major impact on the distribution of carbonate facies, resulting in the percentage of oolitic carbonate being highest on the northeast-facing edges of the platform.

Along with an attempt to understand the spatial (aerial) distribution of carbonates in the SACROC Unit, previous researchers also investigated the variation of carbonates with depth and subsequently divided this Unit into Lower Canyon, Middle Canyon, Upper Canyon, and Cisco Groups through detailed analyses of cores, logging data, and biostratigraphy (fusulinid age) (fig. 3). Their analyses suggested that the Cisco Group, which was characterized as a highly heterogeneous group representing the dramatic changes in depositional environments, unconformably overlies the Canyon Group. The Upper Canyon is a highly porous zone, which includes erosional remnants resulting from a prolonged low sea level. The Middle/Lower Canyon Groups consist of high porosity layers separated by low porosity carbonate muds. More detailed

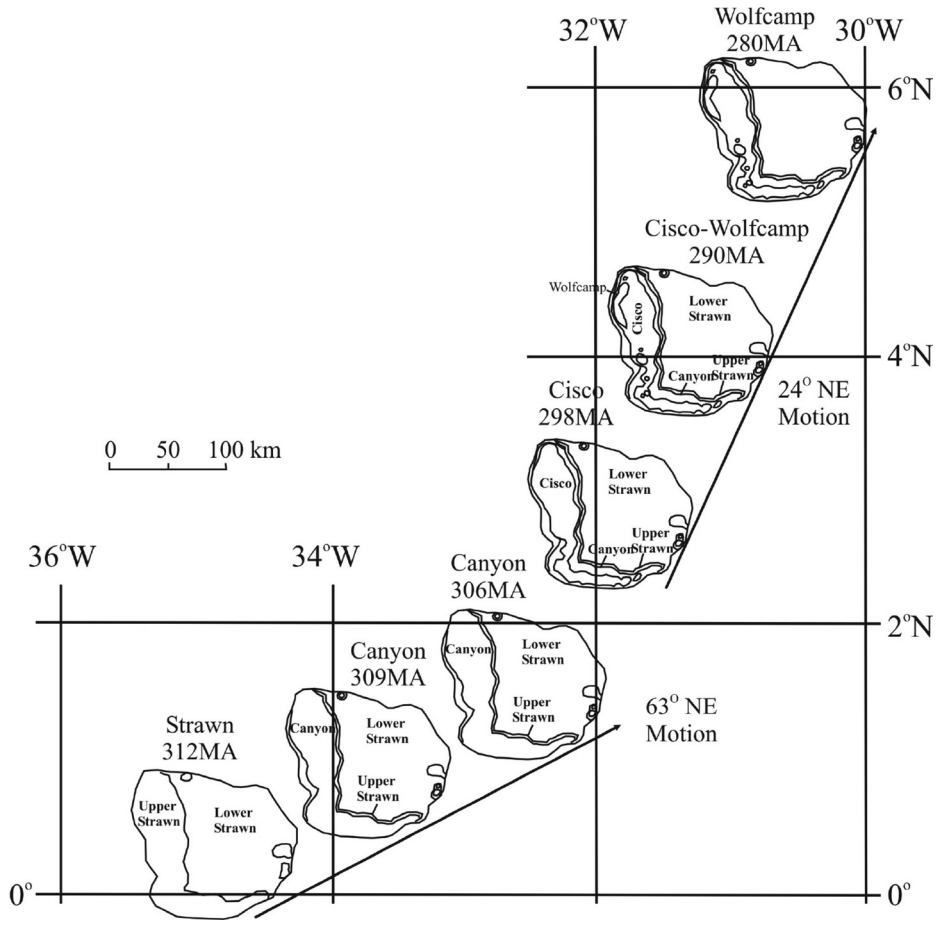

Fig. 2. The paleolatitude and paleogeographic location of the Horseshoe Atoll (Walker and others, 1991).

classification of the stratigraphy in the Cisco and Canyon Groups can be found in Reid and Reid (1991) and Hawkins and others (1996).

Changes in depositional environments show a wide variability of both porosity (0 to 30%) and permeability (0 to 1000 mD) in the Cisco and Canyon Groups (fig. 3). Bergenback and Terriere (1953) megascopically observed porosity distribution and reported values that ranged between approximately 0 to 20 percent. Similarly, Myers and others (1956) reported porosity values from 0 to 30 percent after core analysis. Both found that most porosity is developed during secondary diagenetic processes such as calcitization, dolomitization, and silicification. Burnside (1959) indicated that open fractures markedly influenced the permeability field. Other studies such as Vest (1970), Kane (1979), Langston and others (1988), Raines (2005), and Brnak and others (2006) provided average porosity and permeability, and the reader is referred to these studies for more detailed discussion.

Schatzinger (1988) estimated porosity from analysis of the depositional environment. In this study, the eastern part of the Horseshoe Atoll was spatially divided into three zones. The first zone included the Cogdell field and northern SACROC Unit

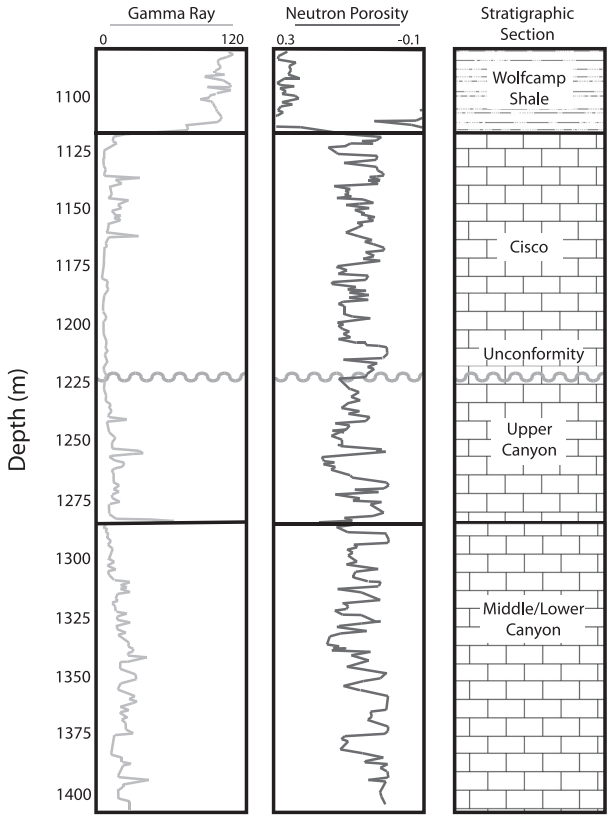

Summary of Previous Studies Estimating Carbonate Rock Properties in Cisco and Canyon Formations

Porosity (%)	Permeability (mD)	References
(0-20)		Bergenback and Terriere (1953)
6 (0-30)	4.5 (0-85), cracks, fractures 2,500	Myers and others (1956)
6	(0-85)	Burnside (1959)
10.3	30.6	Vest, (1970)
3.93	19.4	Kane, (1979)
9.41	3.03	Langston and others (1988)
9.8 (0-22.5)	19 (0.1-1760)	Raines, (2005)
7.6	19.4	Brnak and others (2006)
Sponge mound facies (15-20) Phylloid mound facies (<15) Oolitic grainstone facies (20-30) Peritida mud facies (locally 5) Breccia facies (locally 10)		Schatzinger, (1988)
Oolitic grainstone facies (25-30) Bioclastic grainstone facies (25-30) Algal wackestone facies (15-20)	Oolitic grainstone facies (>100) Bioclastic grainstone facies (10-50) Algal wackestone facies (<10)	Reid and Reid, (1991) Codgell Field

Fig. 3. Well logs representing the SACROC northern platform and summary of previous studies estimating carbonate rock properties in Cisco and Canyon Groups.

(fig. 1B), both reflecting turbulent environments with the deposition of basin-facing ooid shoals. The central and southern SACROC Unit shows intermediate turbulence conditions with the deposition of sponge-algal-bryozoan buildups. Finally, the Diamond M field and southern SACROC Unit reflect a low turbulence environment (fig. 1B). Research by Reid and Reid (1991) was more focused on the Cogdell field. In their work, the carbonate reef limestone was divided into nine zones after fusulinid age-dating and well logging correlations. Recently, there has been a similar effort to build stratigraphic frameworks and porosity distributions from the correlations of fusulinid biostratigraphy in the SACROC Unit (Hawkins and others, 1996). After examination of core and correlation with well logging, Hawkins and others (1996) found that porosity patterns were closely related to changes in depositional facies and suggested that the biostratigraphic distinction was significant in this field.

Injection and Production History

The SACROC Unit was discovered in 1948. The estimated original oil in place (OOIP) was approximated at 2.73 billion Stock Tank Barrels (STB) (Dicharry and others, 1973). From 1948 to 1951, over 1200 production wells were drilled in this Unit (Bayat and others, 1996). During this period, oil was produced by the solution gas drive mechanism resulting in reduction of the original reservoir pressure (3122 psi = 21.53 MPa) by over 50 percent (1560 psi = 11.38 MPa) for only 5 percent of OOIP production (Dicharry and others, 1973; Brummett and others, 1976).

To improve oil production and prevent crippling pressure loss, one of the largest pressure maintenance projects in the United States was started in 1954 (fig. 4). Fifty three water wells initiated water injection at a rate of approximately 21,000 m^3 per day along the crest of the SACROC Unit (Allen and LaRue, 1957; Allen and Thomas, 1959; Dixon and Newton, 1965; Dicharry and others, 1973; Brummett and others, 1976; Bayat and others, 1996). The locations of water injection wells are shown in figure 1C. Before water injection began, only 1 percent of the reservoir was above the bubblepoint pressure (12.45 MPa). After 17 years (until 1971) of water injection, 77 percent of this Unit became above the bubblepoint pressure. The estimated waterflooding front at the end of waterflooding period in 1973 is shown in figure 1C. However, despite the high sweep efficiency of the water injection, approximately 1.2 billion STB of oil still remained in this Unit at the end of the water injection period. In addition, the repressurization plan eventually resulted in high reservoir pressure in the center of the SACROC Unit and low pressure towards the eastern and western margins. Because of the tremendous volume of oil still left in the reservoir after water injection, other enhanced oil recovery techniques were considered to improve oil recovery.

The SACROC field started with primary recovery, or the solution gas drive, then followed this with secondary recovery operations consisting of water-flooding. Based on engineering calculations, in 1972 the SACROC Unit operating committee decided that CO_2 injection would be the best tertiary oil recovery mechanism. The next major task was to find a CO_2 source near the SACROC Unit. The closest CO_2 sources were the Ellenburger hydrocarbon gas power plants in the Val Verde basin, about 220 miles (354 km) south of the SACROC Unit (fig. 1A). However, CO_2 from gas power plants were not ideal sources due to the lack of a consistent supply (gas power plants are subject to potential shutdowns due to their internal problems). Therefore, the SACROC operators switched CO_2 supply from gas power plants to McElmo Dome, a natural CO_2 reservoir in Colorado, in 1996 (Weeter and Halstead, 1982). The detailed characteristics including CO_2 accumulation in the CO_2 natural reservoir of McElmo Dome are discussed in Gerling (1983) and Allis and (2001). By changing the source of CO_2 from the gas power plants to a natural CO_2 reservoir, operations became more stable because of the continuous CO_2

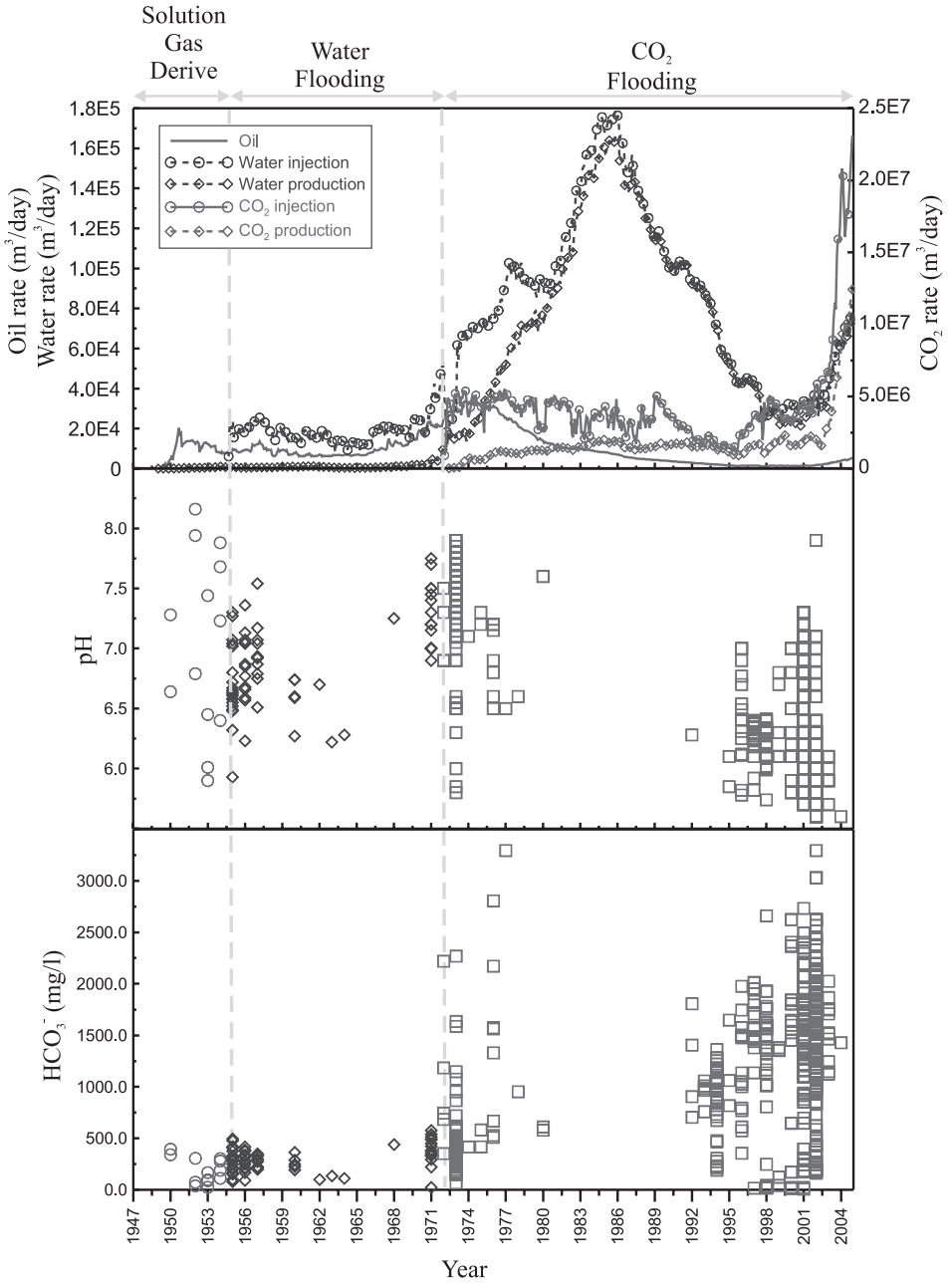

Fig. 4. Injection and production history of oil, water, and CO_2 (Raines, 2007) and corresponding evolution of pH and HCO_3^- in produced water from Cisco and Canyon Groups.

supply. In summary, about 93 million metric tons of CO_2 were injected and about 38 million metric tons were produced from 1972 to 2005 in this Unit. As a result, a simple mass-balance suggests that the site has accumulated about 55 million metric tons of CO_2 (Raines, 2005).

Effect of CO_2 Injection on Reservoir Brine Chemistry

Changes in reservoir brine chemistry due to injection of a massive amount of CO_2 have been observed in field-scale operations (Bowker and Shuler, 1991; Klusman, 2003; Emberley and others, 2004; Kharaka and others, 2006; Mito and others, 2008). These authors found that CO_2 dissolution typically results in the reservoir brine having a lower pH and higher HCO_3^- concentration. Subsequently, these reactions induce changes in reservoir rock properties. For this SACROC case study, we gathered and analyzed the brine chemistry data from the Cisco and Canyon Groups to investigate whether the similar alteration of reservoir brine chemistry, due to 35 years of CO_2 injection, occurred in the SACROC Unit. The brine chemistry data is a compilation of various analyses and reports from the Martin Water Laboratory, Unichem, the Texas Water Board, Permian Production Chemical, and the United States Geological Survey (Bowden, Kinder Morgan CO_2, personal communication, 2006). The statistical classification of these data sets, calculated for each period of differing oil-production mechanisms, is shown in table 1.

Statistics of the SACROC reservoir brine chemistry (table 1) show that mean concentration of Na^+ and Cl^- were respectively 27,292 mg/L and 51,496 mg/L during the solution gas period (1948-1952) and their concentration decreased to 24,750 mg/L and 46,263 mg/L throughout the waterflooding period (1953-1971). This dilution of reservoir brine is the result of relatively fresh water being injected and recycled during the waterflooding period. Similarly, the dilution of reservoir brine during the waterflooding period has been observed in another oilfield, the Rangely Field, Colorado. Brine salinity before waterflooding was approximately 100,000 ppm in Rangely Field but it decreased to 33,000 ppm at the end of waterflooding (Bowker and Shuler, 1991). After the initiation of CO_2 flooding in the SACROC Unit (1972-2004), it was expected that increases of Na^+, Cl^-, and other species' concentrations would occur, similar to the observations made in Rangely Field, Colorado by Klusman (2003). However, mean values of Na^+, Ca^{2+}, Cl^-, and SO_4^{2-} concentrations kept decreasing during the CO_2 flooding period in the SACROC Unit (table 1). We presume that this difference occurred because the SACROC operators performed waterflooding prior to CO_2 injection even during the CO_2 flooding period to increase reservoir pressure to minimum miscibility pressure and also employed Water-Alternating-Gas (WAG) processes. Therefore, huge amounts of water were injected and recycled even in the CO_2 flooding period (fig. 4), and caused the continued dilution of reservoir brine. In addition, the CO_2 injection formation in Rangely Field, Colorado, is sandstone but it is limestone in the SACROC Unit. Therefore, the potential chemistry changes between these two reservoirs due to CO_2 injection are expected to be different.

Evolving patterns of both pH and HCO_3^- concentrations shown in figure 4 are similar to the observations from other field-scale operations (Klusman, 2003; Emberley and others, 2004; Kharaka and others, 2006; Mito and others, 2008). The pH becomes lower and the HCO_3^- concentration increases from the waterflooding period until the CO_2 flooding period. Especially, in the SACROC Unit, where the decrease in pH during CO_2 flooding was small (6.88 to 6.43 shown in table 1) compared with the pH decrease in the Rangely field (6.69 to 5.50; Kluseman, 2003) and Frio field (6.7 to 5.5; Kharaka and others, 2006) where the formation rocks are sandstone. This result suggests that carbonate rock, which is the major rock in the SACROC Unit, buffered the drop in pH. The dramatic increase of HCO_3^- (306.90 to 1313.69 mg/L) is possibly caused by both the injected CO_2 being dissolved in the brine solution and the dissolution of calcite ($CaCO_3$) and dolomite ($CaMg(CO_3)_2$). Notably, the concentration of Mg^{2+} in the reservoir brine increased (917.90 to 1,305.01 mg/L) during the CO_2 flooding period, suggesting that CO_2 injection possibly caused the dissolution of Mg-bearing minerals such as dolomite ($CaMg(CO_3)_2$) and Magnesite ($MgCO_3$).

Table 1

Statistics of water chemistry analyses and chemical modeling of reservoir fluids in Cisco and Canyon Groups during each oil production mechanism

Oil Production Mechanisms		Solution gas	Water flooding	CO_2 flooding
Period (Year)		1948-1952	1953-1971	1972-2004
Number of samples		13	69	758
Reservoir pressure (MPa)		21.50	11.38	16.55
Reservoir temperature (°C)		54.50	54.50	54.50
pH	Mean	7.06	6.88	6.43
	Std.	0.75	0.37	0.60
Na^+ (mg/L)	Mean	27,292.00	24,750.72	24,248.52
	Std.	11,011.07	11,026.97	9,192.98
Ca^{2+} (mg/L)	Mean	4,238.15	3,613.78	2,675.24
	Std.	2,256.80	2,065.09	1,644.09
Mg^{2+} (mg/L)	Mean	959.92	917.90	1,305.01
	Std.	444.99	464.05	833.68
Cl^- (mg/L)	Mean	51,496.46	46,263.46	44,587.90
	Std.	21,838.31	21,068.02	16,665.64
HCO_3^- (mg/L)	Mean	185.15	306.90	1313.69
	Std.	125.06	112.78	675.52
SO_4^{2-} (mg/L)	Mean	1,675.31	1,050.61	782.80
	Std.	755.17	697.64	679.30
CO_2 fugacity (MPa)	Mean	3.64* (0.0169)	3.35** (0.0294)	67.68*** (0.4089)
	Std.	3.77*	1.72**	54.36***
SI of calcite	Mean	0.68	0.80	0.62
($CaCO_3$)	Std.	0.92	0.47	0.78
SI of dolomite	Mean	2.28	2.55	2.44
($CaMg(CO_3)_2$)	Std.	1.81	0.95	1.51
SI of Magnesite	Mean	0.13	0.28	0.35
($Mg(CO_3)$)	Std.	0.89	0.49	0.80
SI of anhydrite	Mean	-0.43	-0.69	-1.00
($CaSO_4$)	Std.	0.26	0.26	0.46
SI of gypsum	Mean	-0.57	-0.83	-1.14
($CaSO_4 \cdot H_2O$)	Std.	0.27	0.26	0.46

*, **, and *** is respectively calculated with reservoir pressure 21.5, 11.38, and 16.55 MPa because reservoir pressure varies historically (Dicharry and others, 1973; Brummett and others, 1976). Parentheses indicate the normalized CO_2 fugacity at 0.1 MPa. Reservoir temperature is from Langston and others (1988). SI represents the saturation index of mineral.

CO_2 fugacity can be an indicator as to whether injected CO_2 was dissolved in the reservoir brine, and the Saturation Indexes (SI) of minerals can provide key information associated with the degree of mineral saturation in the reservoir brine. Therefore, CO_2 fugacity and SI of representative carbonate and sulfate minerals are calculated with the B-dot activity coefficient model (Helgeson, 1969) using Geochemist's Workbench (GWB™) version 7.0 (Bethke, 1996). The statistics for the modeled CO_2 fugacity in table 1 show that the mean of modeled CO_2 fugacity is similar throughout the solution gas (3.64 MPa) and waterflooding (3.35 MPa) periods. However, the mean value of the modeled CO_2 fugacity significantly increased to 67.68 MPa during the CO_2 flooding period showing the evidence of CO_2 dissolution in reservoir brine. The

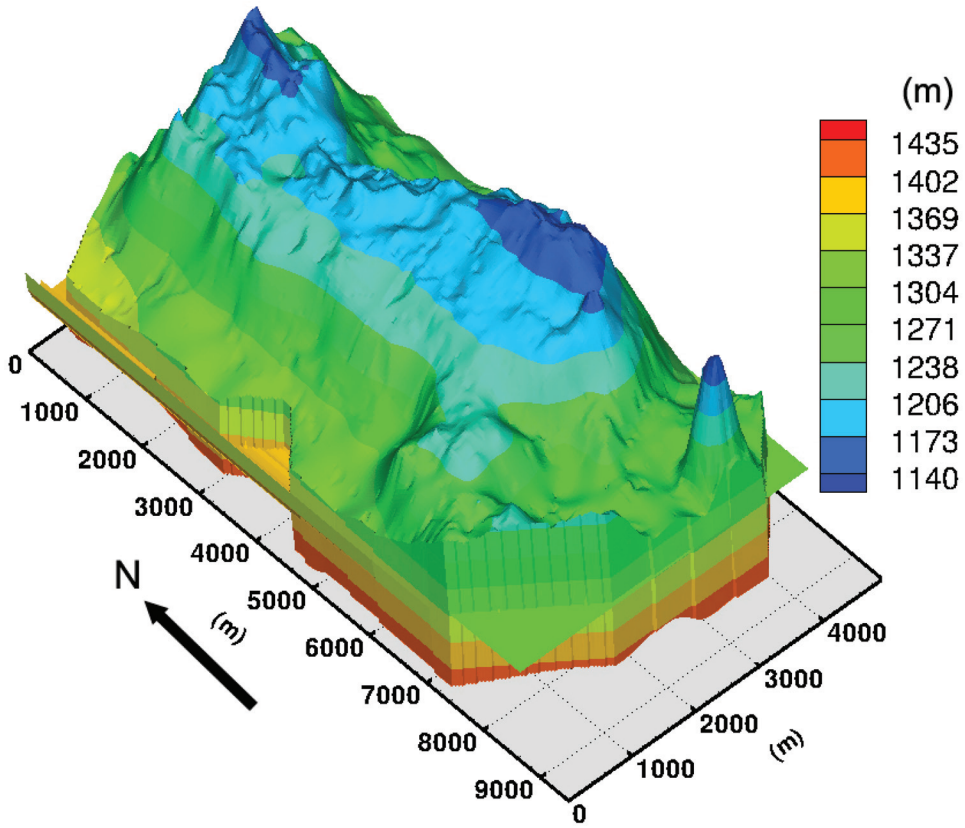

Fig. 5. Structure of 3-D geocellular model representing Cisco and Canyon Groups in the SACROC northern platform. Label (m) indicates the formation depth from the sea level.

modeled SI values suggested that the reservoir brine in the Cisco and Canyon Groups was oversaturated with carbonate minerals but it was undersaturated with anhydrite and gypsum during the entire oil production period (1948-2004). Although the chemistry of the dissolved species in the reservoir brine evolves during oil production periods (fig. 4 and table 1), the saturation states of minerals did not significantly vary, suggesting that chemical reactions between dissolved species are relatively faster than water-rock interaction. In addition, this analysis also suggests that 35 years is not enough time to predict definite changes of mineral saturation states.

Description of 3-D, high-resolution geocellular model in SACROC northern platform and upscaling

The 3-D geocellular model representing the Cisco and Canyon Groups in the SACROC northern platform is illustrated in figure 5. The approximate size of the model is 4,000 m wide and 10,000 m long. The top of the geocellular model shows the upper configuration of the Cisco Group, which is approximately 1200 m below sea level, and the bottom of the model shows the lower configuration of the Canyon Group, which is a depth of approximately 1400 m below sea level.

Figures 6A–D show the external and internal distributions of both porosity and permeability. In this model, porosity distributions were defined from both 3-dimensional seismic surveys and 368 well logging analyses. Subsequently, permeability

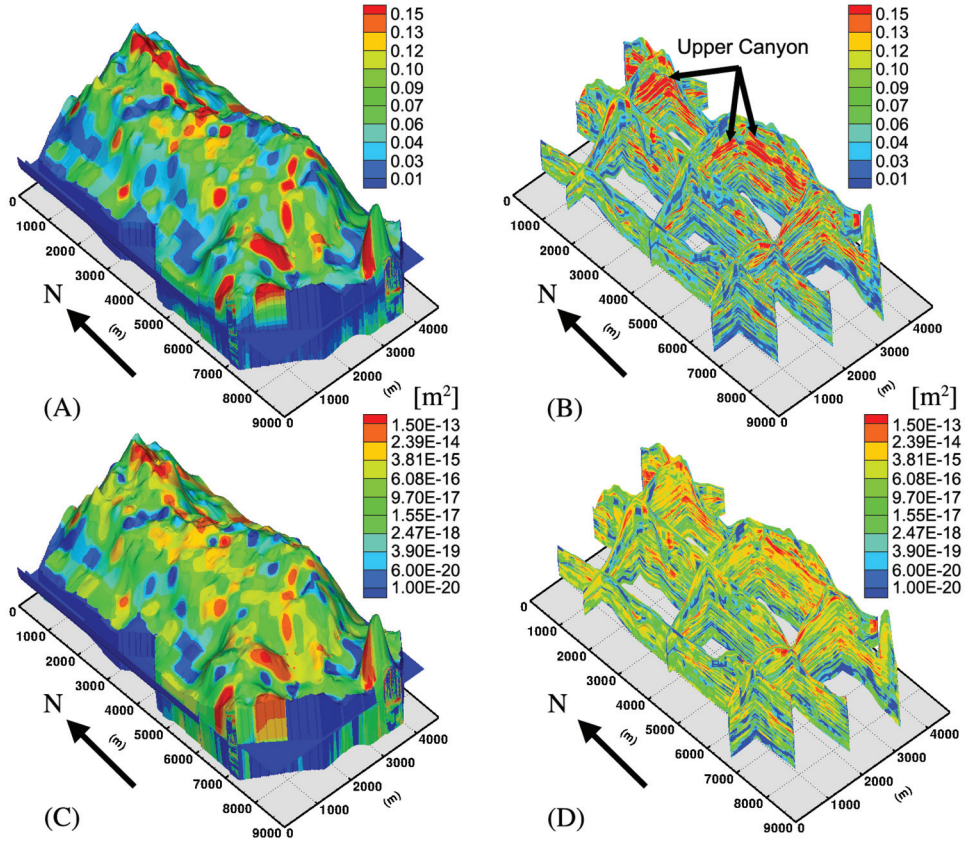

Fig. 6. Internal and external distributions of porosity and permeability in the 3-D geocellular model: (A) external distribution of porosity, (B) internal distribution of porosity, (C) external distribution of permeability (m^2), and (D) internal distribution of permeability (m^2).

distributions were calculated from seismically calibrated porosity distributions using empirical equations derived from rock fabric classification (Lucia and Kerans, 2004). The global transforming equation has been derived for carbonate rock as (Lucia, 1995, 1999; Jennings and Lucia, 2003):

$$\log(k) = (9.792 - 12.0838\log(\lambda)) + (8.6711 - 8.2965\log(\lambda))\log(\phi) \qquad (1)$$

where, λ, k, and ϕ are, respectively, rock-fabric number, permeability, and interparticle porosity. Specifically, λ represents the specific class of carbonate rock based on petrophyiscal properties such as inter-particle porosity in tandem with geological descriptions of particle size and sorting. Lucia and Kerans (2004) applied this equation to estimate the permeability distribution in the SACROC northern platform. The detailed parameters of rock-fabric numbers in this model are described in table 2.

This 3-D geocellular model preserves the detailed heterogeneity variation of both porosity and permeability (figs. 6A-D). The model reveals that the Cisco and Canyon Groups typically lie within a "stacked system" of alternating high and low porosity layers (fig. 6B). The thick and high porous zone shown in figure 6B represents the Upper Canyon Group. The Cisco Group is located above the Upper Canyon Group, and the Middle/Lower Canyon Groups are below the Upper Canyon Group. Specifically, the

Table 2

Permeability estimation using porosity and rock-fabric number (Lucia and Kerans, 2004)

Formation	Sequence	Rock- fabric number (λ)	Transforming equations	
Cisco	1	Reduced major axis transformation	$\boldsymbol{k} = 2.1625\times10^{6}\times\phi^{3.8844}$	Highest portion of Cisco (Implication of karsting)
	2	1.7	$\boldsymbol{k} = 1.031\times10^{7}\times\phi^{6.7592}$	Late Cisco (wide variety of rock fabrics)
	3	1.9	$\boldsymbol{k} = 2.69\times10^{6}\times\phi^{6.3584}$	Early Cisco (Characterized by fusulinid/crinoidal/peloid grain dominated packstones, grainstones, and wackestones
Canyon	1	2.5	$\boldsymbol{k} = 97628\times\phi^{5.3696}$	Early Canyon: (Characterized by moldic ooid grainstone, grain-dominated packstone, and mud-dominated fabrics)
	2	1.75	$\boldsymbol{k} = 38520\times\phi^{5.0923}$	Late Canyon: (Characterized by crinoidal/fusulinid/peloid, grain-dominated packstones, and mud-dominated fabrics having vuggy porosity)

Middle/Lower Canyon Groups consist of several layered high porosity zones separated by low-porosity carbonate mud.

The 3-D geocellular model describing the Cisco and Canyon Groups includes 9,450,623 (149 × 287 × 221) elements (figs. 5 and 6). Although the model provides a quantified characterization of the natural heterogeneity of both porosity and permeability distributions in the SACROC northern platform, the utilization of this model in describing CO_2 trapping mechanisms was hampered due to the large number of elements; only supercomputers capable of massively parallel computation can accommodate simulations of this model. For this reason, we elected to upscale the model to fewer elements. Such upscaling invariably results in a loss of heterogeneity resolution, but we tried to preserve as much of this heterogeneity as possible. The purpose of upscaling was two-fold: (1) about 9.4 million elements exceeded the memory capacity of our model simulators on a personal computer and (2) the original porosity and permeability data as estimated from geophysical data varied extremely from cell-to-cell, sometimes as much as several orders of magnitude in permeability. Upscaling smoothes these data through the averaging process and facilitates a more stable numerical solution, albeit with the loss of heterogeneity resolution.

In this study, porosity is upscaled by the volumetric averaging technique, and permeability (k) is upscaled with an algorithm developed through an equivalent resistor network model (King, 1989). The upscaling equation and conceptual diagram used in this work is shown in eq 2 and figure 7, respectively.

$$k_{eff} = \frac{4(k_1 + k_3)(k_2 + k_4)[k_2k_4(k_1 + k_3) + k_1k_3(k_2 + k_4)]}{[k_2k_4(k_1 + k_3) + k_1k_3(k_2 + k_4)[k_1 + k_2 + k_3 + k_4] + 3(k_1 + k_2)(k_3 + k_4)(k_1 + k_3)(k_2 + k_4)]} \quad (2)$$

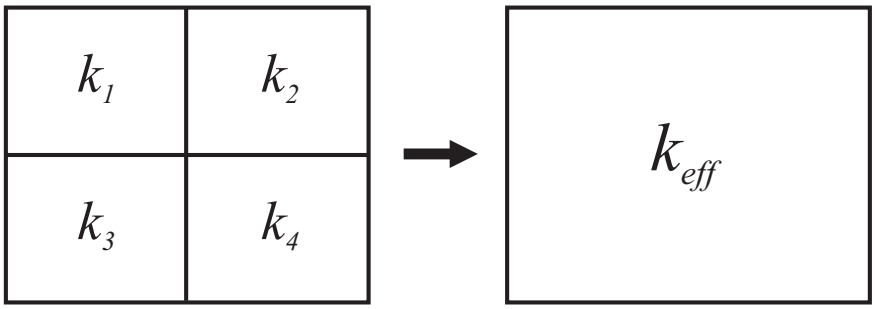

Fig. 7. Upscaled permeability using renormalization and the equivalent equation is shown in eq 2.

This technique is generally called "renormalization" because it successively upscales the symmetric grid-blocks using self-repetitive geometry until the final grid-block size is reached. Using this approach is fast and computationally cheap because it does not require solutions to the differential equations. In addition, it is not constrained by the number of grid-blocks. Because of these practical advantages, many researchers have studied and updated renormalization techniques (Hinrichsen and others, 1993; King, 1996; Gautier and Noetinger, 1997; Renard and others, 2000). Despite its many advantages, renormalization has several drawbacks. If there is a high contrast between neighboring permeability values, using this approach will underestimate the upscaled permeability value (King, 1989; Renard and de Marsily, 1997). In addition, this method has some limitations with respect to applicable boundary conditions (Malick, ms, 1995). Finally, renormalization is specially designed for orthogonal grids. Although our model satisfies several conditions to apply this renormalization technique, the grid is not completely orthogonal. The grid is orthogonal in both the x- and y-direction; however, the z-direction is irregular, which could induce some error in the resulting upscaled permeability. It is extremely difficult to quantify the error due to this non-orthogonality, although we estimate the accrued error to be less than the uncertainty associated with seismic and well logging data used to calibrate the model.

Sequential results of permeability distributions by renormalization are shown in figure 8. In addition, the detailed statistics of permeability values, the number of grid-blocks, and their sizes are shown in table 3. As the grid is upscaled, the size of grid-block becomes greater, and both the means (arithmetic, harmonic, and geometric) and standard deviation of the permeability become smaller. Decrease in the means of upscaled permeability suggests that low permeability values have a greater influence on the calculation of upscaled permeability values. Similarly, decrease in standard deviation of upscaled permeability suggests that permeability distribution from cell-to-cell becomes smoother. Finally, for the model development utilized for the simulation of CO_2 trapping mechanisms in the SACROC northern platform, we obtained the upscaled grid with 15,470 elements shown in figure 8D.

Determination of Boundary Conditions: Evaluation of Wolfcamp Shale Formation as a Suitable Seal

To evaluate the seal integrity of the Wolfcamp Shale Formation, we gathered and analyzed the available water chemistry data to determine the potential sealing effect of this formation. These chemical analyses do not provide definitive proof to whether or not CO_2 leaks through the Wolfcamp Shale Formation because the SACROC Unit comprises a huge area, 356 km^2 (fig. 1). Even the most detailed datasets will not cover

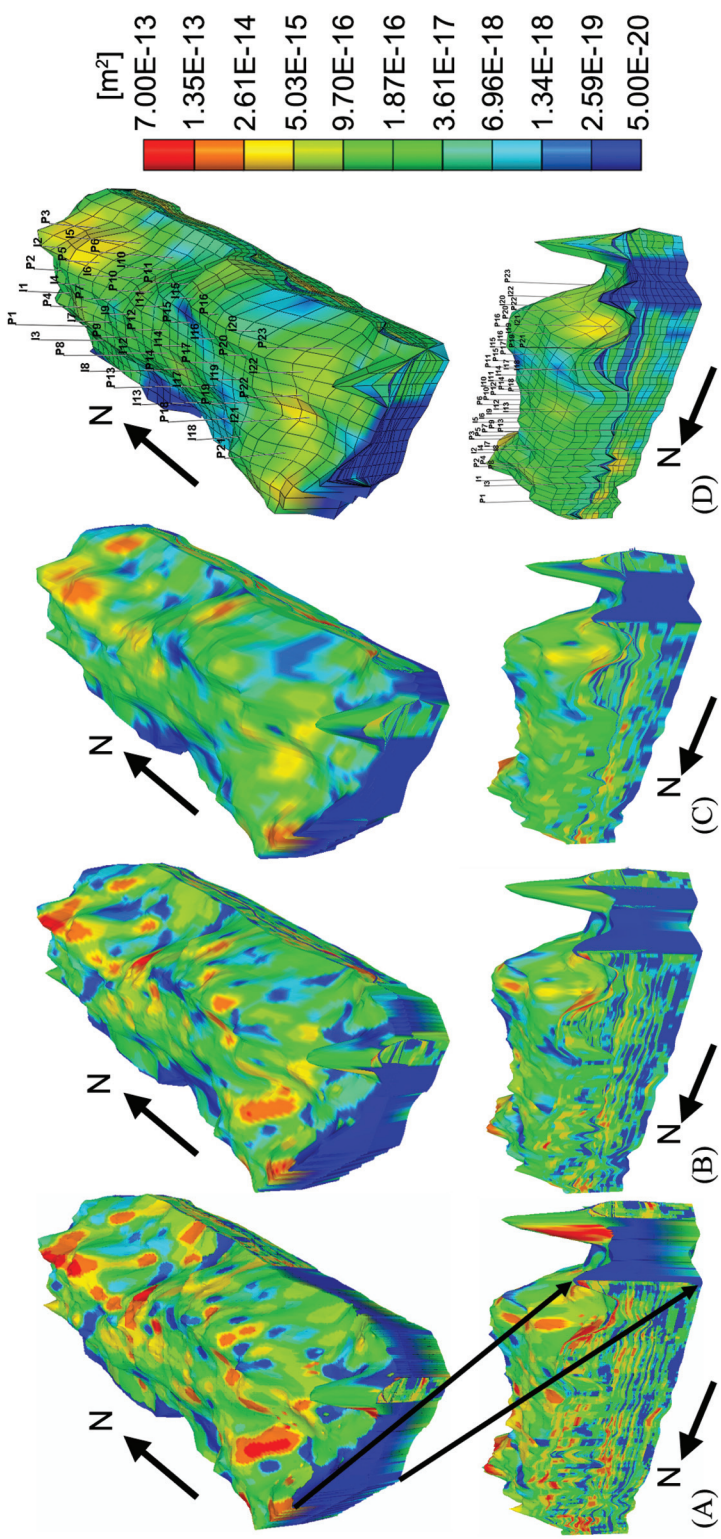

Fig. 8. Internal and external permeability distributions during each renormalization procedure. The detailed grid statistics are shown in table 2: (A) 149×287×221=9,450,623 elements, (B) 74×143×110=1,164,020 elements, (C) 36×71×54=139,968 elements, and (D) 17×35×26=15,470 elements.

Table 3

Detailed statistics of permeability, grid dimensions, and size of grids during the renormalization process

	Number of Grid			Total	Grid size (m)			Permeability (m^2)			
	X	Y	Z	number of Grids	X	Y	Z	Mean			Std. dev.
								Arithmetic	Harmonic	Geometric	
1	149	287	221	9,450,623	30.54	30.46	vary	5.62E-15	8.75E-20	2.13E-18	4.20E-14
2	74	143	110	1,164,020	61.08	60.91	vary	3.58E-15	8.46E-20	1.58E-18	2.40E-14
3	36	71	54	139,968	122.16	121.83	vary	1.93E-15	8.21E-20	1.12E-18	1.38E-14
4	17	35	26	15,470	244.32	243.66	vary	5.10E-16	7.45E-20	5.76E-19	3.26E-15

the entire area of SACROC Unit. As such, the ultimate goal of these analyses is to evaluate the overall performance of the Wolfcamp Shale Formation and evaluate the likelihood that the Wolfcamp Shale Formation currently acts as a suitable seal in this area.

During the geologic time period, the Wolfcamp Shale Formation about 150 m thick was the caprock overlying the hydrocarbon in the Cisco and Canyon Groups (Vest, 1970; Raines and others, 2001). Although CO_2 has been injected during the last 35 years, previous researchers have not reported any indication of CO_2 leakage such as travertine deposits at the surface, changes of shallow groundwater chemistry, anomalous CO_2 gas concentration at the surface, or changes in surface vegetation over time. In addition, several scientific investigations supported the premise that the Wolfcamp Shale Formation might be a suitable seal within the SACROC Unit. For example, Carey and others (2007) measured vertical permeability of the Wolfcamp Shale Formation and suggested that it is low enough (<0.05 mD) to build a capillary barrier that hampers buoyancy-driven migration of CO_2. In addition, their mineralogical and isotopic (oxygen and carbon) analyses suggested that the carbonates in the Wolfcamp Shale Formation appear to be derived from primarily diagenetic processes, supporting that CO_2 is effectively trapped in the Cisco and Canyon Groups.

For this study, we gathered and analyzed the available water chemistry data to determine the potential sealing efficacy of the Wolfcamp Shale Formation. Detailed statistics of brine samples (840) gathered from the Cisco and Canyon Groups are shown in table 1, and those for shallow groundwater samples (170) gathered from the Dockum formation above the Wolfcamp Shale Formation are summarized in table 4. A Piper diagram analysis in Han (ms, 2008) illustrated that the chemistry of the shallow groundwater is distributed from Na-HCO_3 to Ca-HCO_3 while most of the brine is the Na-Cl type.

With a similar approach to analyzing reservoir brine as described in the previous section, "*Effect of CO_2 Injection on Reservoir Brine Chemistry*", we calculated the CO_2 fugacity and saturation indexes (SI) of minerals from shallow groundwater. Interestingly, mean values of CO_2 fugacity from the shallow groundwater did not change from water flooding to CO_2 injection period (table 4), suggesting that CO_2 injection into the Cisco and Canyon Groups did not significantly impact the chemistry of the shallow groundwater above the Wolfcamp Shale formation. In addition, SI analysis suggests that shallow groundwater is oversaturated with respect to calcite and dolomite, but the degree of oversaturation in the shallow groundwater is smaller than that in the reservoir brine of Cisco and Canyon Groups.

We hypothesized that the concentrations of reservoir brine in the Cisco and Canyon Groups and shallow groundwater above the Wolfcamp Shale Formation would

TABLE 4

Statistics of water chemistry analyses and chemical modeling of shallow groundwater above Wolfcamp Shale Formation (Dockum aquifer) during each oil production mechanism

Oil Production Mechanisms		Solution gas	Waterflooding	CO_2 flooding
Period (Year)		1948-1952	1953-1971	1972-2004
Number of samples		No sample	48	122
Temperature (°C)	Mean		20.85	21.03
	Std.		0.67	1.15
pH	Mean		7.48	7.63
	Std.		0.47	0.68
Na^+ (mg/L)	Mean		278.98	349.26
	Std.		383.12	1009.94
Ca^{2+} (mg/L)	Mean		104.18	125.67
	Std.		130.81	126.47
Mg^{2+} (mg/L)	Mean		46.03	40.92
	Std.		65.08	41.86
Cl^- (mg/L)	Mean		336.13	484.66
	Std.		631.31	1552.49
HCO_3^- (mg/L)	Mean		323.27	304.09
	Std.		105.38	81.21
SO_4^{2-} (mg/L)	Mean		292.16	284.57
	Std.		461.91	421.18
SiO_2(aq) (mg/L)	Mean		22.15	25.17
	Std.		11.26	10.53
CO_2 fugacity (MPa)	Mean		0.009	0.009
	Std.		0.007	0.010
SI of calcite	Mean		0.08	0.45
($CaCO_3$)	Std.		0.44	0.49
SI of dolomite	Mean		0.91	1.53
($CaMg(CO_3)_2$)	Std.		0.87	1.00
SI of Magnesite	Mean		-0.83	-0.58
($Mg(CO_3)$)	Std.		0.46	0.53
SI of anhydrite	Mean		-2.24	-2.03
($CaSO_4$)	Std.		0.81	0.71
SI of gypsum	Mean		-2.01	-1.80
($CaSO_4 \cdot H_2O$)	Std.		0.81	0.71

CO_2 fugacity is calculated with a pressure of 0.1 MPa. SI represents the saturation index of mineral.

show the evidence of a mixing effect if CO_2-saturated reservoir brine leaked through highly permeable conduits such as faults or fractures in the Wolfcamp Shale Formation. The flow system in the Cisco and Canyon Groups are advection-dominant due to a significant alteration of pressure by injection and production activities. Such conditions may accelerate the migration of reservoir brine through highly permeable conduits with the result that CO_2-saturated reservoir brine may make its way to the above shallow groundwater zone.

To evaluate the potential chemical signatures of such mixing effects, we simulated equilibrium mixing with mean values of dissolved species from both reservoir brine and shallow groundwater collected during CO_2 flooding periods (tables 1 and 4),

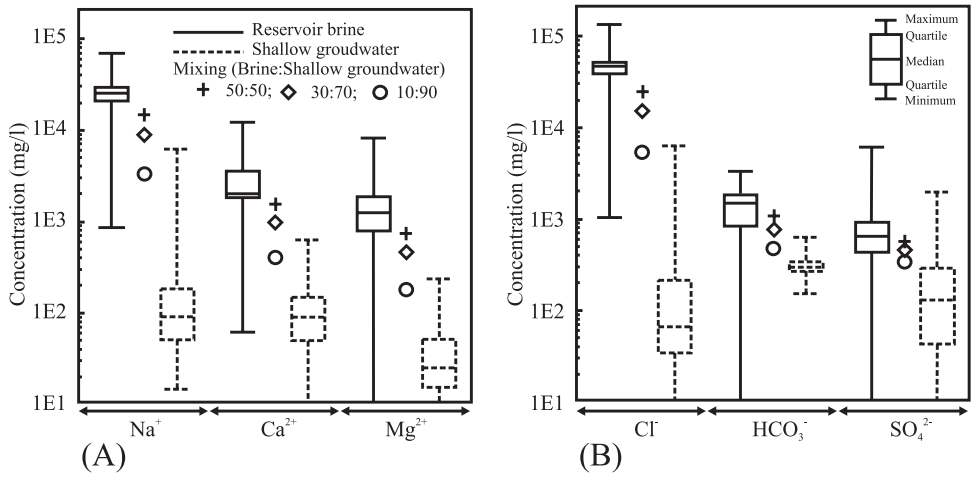

Fig. 9. Box-and-whisker diagram showing the range of brine and shallow groundwater, and results of equilibrium mixing model simulated after varying the volume of reservoir brine (10, 30, and 50%).

using PHREEQC version 2.15.0 with thermodynamic data known as phreeqc.dat (Parkhurst and Appelo, 1999). Three sets of mixing models were simulated after varying the volume of reservoir brine (10, 30, and 50%). The simulation results are plotted in the Box-Whisker plot between concentrations of individual species in the reservoir brine and shallow groundwater (fig. 9). The plot shows that concentrations of dissolved species between reservoir brine and shallow groundwater are typically different and generally provide no distinct indication of communication. However, results of the equilibrium mixing model show that a few shallow groundwater samples potentially show the mixing effect with reservoir brine. Results of 10 percent-brine mixing simulations (circle in fig. 9) are plotted within the range of both brine and shallow groundwater. In detail, less than 5 percent of shallow groundwater samples have a concentration greater than the modeled concentration of the 10 percent-brine mixing model. This analysis suggests that a few shallow groundwater samples might be locally contaminated with reservoir brine. However, it is difficult to conclude that the contamination of shallow groundwater is mainly due to the leakage of CO_2-saturated reservoir brine through the Wolfcamp Shale Formation. In the SACROC Unit, there exist many brine pits on the surface used to store recycled reservoir brine. Therefore, it is possible that this stored reservoir brine on the surface could recharge downward into the shallow groundwater zones and induce the contamination of shallow groundwater.

Based on the analysis of brine and shallow groundwater chemistry, we concluded that the Wolfcamp Shale Formation generally acts as a suitable seal in the SACROC Unit. Previous results of CO_2 fugacity calculation showed that there was no significant increase of modeled CO_2 fugacity in shallow groundwater (table 4) although the modeled CO_2 fugacity of reservoir brine in the Cisco and Canyon Groups significantly increased during the CO_2 flooding period. In addition, the equilibrium mixing model shows that only less than 5 percent of shallow groundwater samples displays the evidence of mixing effects with reservoir brine. Even then, it is also possible that this mixing is due to the downward recharge of recycled brine from brine pits at the surface during enhanced oil recovery.

Sources and sinks: actual CO_2 injection and production histories

We analyzed CO_2 injection and production histories provided by Kinder Morgan CO_2 Inc. in the SACROC northern platform. According to these records,

97 wells were used as CO_2 injectors at the SACROC northern platform from 1972 to 2002. Among them, 51 wells were actively used to inject about 13 million metric tons of CO_2 (13,048,845,748 kg) into Cisco and Canyon Groups. Another 219 wells were used as CO_2 producers during the same period. Among them, 124 wells were actively used to produce about 6 million metric tons of CO_2 (6,104,258,074 kg). A simple mass-balance suggests a net of about 7 million metric tons of CO_2 (6,944,587,674 kg) are sequestered in the SACROC northern platform.

Analysis of Competing CO_2 Trapping Mechanisms at SACROC Northern Platform

We developed two different models representing CO_2 trapping mechanisms at the SACROC northern platform, both utilizing the hydrogeologic framework, boundary conditions, and sources/sinks described above. The objective of these two simulations was to predict and compare the major trapping mechanisms, including hydrostratigraphic, residual, brine-solubility, oil-solubility, and mineralization.

The first model was designed for simulating CO_2 trapping mechanisms in a reservoir saturated with brine only. The other model was designed for simulating CO_2 trapping mechanisms in a reservoir saturated with both brine and oil. The latter model provides a relatively realistic representation of CO_2 trapping mechanisms in the SACROC field because this field is a petroleum reservoir subjected to a long history of CO_2 injection for enhanced oil recovery. We conducted all simulations during a 200-year time period from 1972 to 2172. All simulations were performed with the CMG's GEM simulator, a multi-dimensional, finite-difference, isothermal compositional simulator (Computer Modeling Group, 2008).

SACROC CO_2 Trapping Model—Brine Only

Initial conditions.—From 1954 to 1971, water was injected in a centerline pattern to increase the reservoir pressure above bubblepoint pressure (12.45 MPa) as illustrated in Dicharry and others (1973) and Langston and others (1988). As a result, when CO_2 injection began in 1972, reservoir pressure had risen above 16.55 MPa. This pressure condition is assigned as the initial average reservoir pressure (16.55 MPa) in the upscaled geocellular model with 15,470 ($=17\times35\times26$) elements shown in figure 8D. To achieve this average pressure, reservoir pressure was assigned as hydrostatic pressure from the formation top equal to 15.73 MPa to the bottom pressure equal to 17.90 MPa in the upscaled model. Langston and others (1988) reported the reservoir temperature as 54.5°C, and we used this value as an average reservoir temperature. In the model, the initial reservoir temperature was assigned using a conductive gradient with temperature at the top equal to 54.35°C and bottom equal to 59.83°C. The assigned temperatures in the model remain constant during the simulation period although there could be an occurrence of a non-isothermal effect caused by CO_2 injection and migration. We refer readers to other studies about the detailed non-isothermal effect related to CO_2 sequestration processes (Bielinski and others, 2008; Lu and Connell, 2008; André and others, 2010; Han and others, 2010b).

Boundary conditions.—Through rigorous analysis of water chemistry data, we were able to predict a possibility of local contamination of shallow groundwater caused by either surface recharge of recycled brine or leakage of CO_2-saturated brine through the Wolfcamp Shale Formation. Local brine-contamination notwithstanding, we assume that the Wolfcamp Shale Formation is a sufficient sealing unit. Some observations that justify this assumption include

(1) The Wolfcamp Shale Formation, as thick as 150 m, was a seal for hydrocarbon in the Cisco and Canyon Groups during vast periods of geologic time (Vest, 1970; Raines and others, 2001).
(2) Measured vertical permeability (k_z) in the Wolfcamp Shale Formation is low (<0.05 mD) enough to prevent vertical CO_2 migration according to Carey and others (2007).
(3) X-ray diffraction analysis suggests that carbonate minerals in the Wolfcamp Shale formation appear to derive from primarily diagenetic processes and their isotope compositions show typical marine-originated $\delta^{13}C$ values (Carey and others, 2007).
(4) CO_2 fugacity in reservoir fluids of Cisco and Canyon Groups significantly increases during the CO_2 injection period (table 1) but CO_2 fugacity does not vary in shallow groundwater above the Wolfcamp Shale Formation (table 4).

As such, we assigned a no-flow condition at the upper boundary in the 3-D upscaled geocellular model. Although both Kaszuba and others (2005), Xu and others (2005), and Busch and others (2008) indicate that the caprock can also act as a reactive component and contribute to mineralization, we think that the role of the caprock as a reactive component is not significant since the flow mechanism in the caprock is dominantly diffusion-driven. Gaus and others (2005) concluded that the mineralization due to diffusion in typical seals occurs in the lower 2 m after 3000 years. Similarly, Lu and others (2009) measured carbon isotopes from mudrock seal immediately above a natural CO_2-rich reservoir in the North Sea Miller oil field and suggested that CO_2 migrated only 12 m through mudrock seal during 70 to 80 million years. As described, the mineralization within such caprocks will be much smaller than that in the targeted reservoir formations. Therefore, treating the seals as no-flow boundaries will not significantly affect the prediction of CO_2 trapping mechanisms and capacity estimation.

Due to these reasons, the eastern, western, and northern boundaries are treated as no-flow boundaries because the Wolfcamp Shale Formation meets these boundaries; the carbonate reef complex of the Cisco and Canyon Groups is prism-shaped (Vest, 1970). The bottom boundary is also designated as a no-flow boundary because the Strawn Formation below the Cisco and Canyon Groups is also a low permeable unit (Raines, Kinder Morgan CO_2 Inc., personal communication, 2006). Finally, a hydrostatically constant pressure condition known as the "Dirichlet" condition is assumed at the southern boundary of the model because this boundary is connected to the middle part of the SACROC Unit (fig. 1C).

Transport and chemistry input data.—Relative permeability curves of supercritical-phase CO_2 ($k_r^{CO_2}$) and brine (k_r^{br}) in the 3-D geocellular model were developed by extrapolating $k_r^{CO_2}$ data measured by Bennion and Bachu (2005). They measured $k_r^{CO_2}$ and k_r^{br} in a 0.16 m core of low-permeability carbonate rock collected from Wabamun Lake, with experimental conditions of 41°C and 22.4 MPa. Hysteretic effects were included in the $k_r^{CO_2}$ curve using a modified Land equation (Land, 1968; Kumar and others, 2005; Han and others, 2010a).

$$k_r^{CO_2}(S_{CO_2}) = k_r^{CO_2}(S_{CO_2}) \text{ during drainage} \tag{3}$$

$$k_r^{CO_2}(S_{CO_2}) = k_r^{CO_2}(S_{CO_2}(shifted)) \text{ during imbibition} \tag{4}$$

Where

$$S_{CO_2}(shifted) = \frac{S_{CO_2} - S_{grh}}{S_{gh} - S_{grh}} S_{gh} \tag{5}$$

Table 5

Volume fractions, surface areas, and kinetic rates assigned in the upscaled geocellular model

Mineral	Weight percent (Carey, 2007)	Modified weight percent	Volume fraction	Surface area (m^2/m^3)	Activation energy (J/mol)	$Logk_{25}$ (mol/m^2s)	Model kinetic rate
Calcite	0.82	0.62	0.6063	586.72	41870	-8.80	Svensson and Dreybrodt, (1992)
Dolomite	0	0.1	0.0933	559.86	41870	-9.22	White, (2005)
Kaolinite	0.01	0.01	0.0110	6115.38	62760	-13.00	Nagy, (1995)
Anhydrite	0	0.1	0.0892	535.35	41870	-8.80	Same as calcite
Quartz	0.03	0.03	0.0303	606.87	87500	-13.90	Tester and others, (1994)
Illite	0.02	0.02	0.0193	5781.82	58620	-14.00	Knauss and Wolery, (1989)
Ankerite	0.12	0.12	0.1043	521.31	41870	-10.22	Estimated from Dolomite
Dawsonite	0	0	0	657.02	62760	-9.09	Hellevang, (2005)
Siderite	0	0	0	401.52	41870	-10.22	Estimated from Dolomite

and

$$\frac{1}{S_{gr}^{\max}} = \frac{1}{S_{grh}} - \frac{1}{S_{gh}} + 1 \tag{6}$$

S_{gh} is the value of S_{CO_2} when the shift to imbibition occurs. S_{grh} is the value of S_{gr} corresponding to S_{gh}. Adopting the Land equation requires the determination of maximum residual saturation ($S_{gr}^{\max}$). An empirical formulation ($S_{gr}^{\max} = 0.5473 - 0.969\phi$) determining $S_{gr}^{\max}$ from porosity (ϕ) was proposed by Holtz (2002). Using this empirical formulation, $S_{gr}^{\max}$ was calculated as 0.4 in this model. Capillary pressure curve for brine and supercritical-phase CO_2 was also developed by extrapolating data measured by Bennion and Bachu (2006). Here, for simplification, the same capillary pressure curve is used for both drainage and imbibition conditions, and the scaling of capillary pressure curve dependent on heterogeneous permeability field (Leverett, 1941; Durmore and Schols, 1974) is not implemented. We refer readers to Plug and Bruining (2007) and Saadatpoor and others (2010) for this specific topic in relation to geologic CO_2 sequestration. Both CO_2 density and viscosity were respectively calculated from the Peng-Robinson equation of state (Peng and Robinson, 1976) and Jossi and others (1962). CO_2 solubility was calculated using Henry's law (Li and Nghiem, 1986) adjusted for the effects of temperature (Harvey, 1996), salinity, and salting out (Bakker, 2003). Drying out effects due to brine evaporation at the vicinity of injection wells was not considered in this work since our primary objective was to identify CO_2 trapping mechanisms at a reservoir scale. We refer readers to other studies for discussion of salt precipitation effects near CO_2 injection wellbores due to drying out processes (André and others, 2007; Giorgis and others, 2007; Pruess and Müller, 2009) and studies of mutual solubility (Duan and Sun, 2003; Spycher and others, 2003). Finally, density and viscosity of the CO_2-H_2O aqueous mixtures with the effects of brine concentration were estimated using data and relationships discussed by Rowe and Chou (1970) and Kestin and others (1981), respectively.

We assigned mineralogy in the 3-D upscaled geocellular model based on X-ray diffraction analyses results (table 5) measured by Carey and others (2007) who analyzed core samples collected from Cisco and Canyon Groups. In their analyses, dolomite and anhydrite were not detected. However, previous geological studies described in Section "*Geologic Descriptions*" indicated that the Cisco and Canyon Groups

were highly altered by calcitization and dolomitization processes and included minor amounts of anhydrite, dolomite, sand, and shale (Bergenback and Terriere, 1953; Myers and others, 1956; Raines and others, 2001). Therefore, we modified mineralogy to include dolomite and anhydrite (table 5).

Geologic studies suggest that dawsonite specifically is considered to be a late-stage mineral deposited in natural CO_2 reservoirs (Baker and others, 1995; Moore and others, 2005). Due to this reason, the possibility of dawsonite precipitation during CO_2 sequestration processes has been studied with various experiments (Kaszuba and others, 2005; Hellevang and others, 2005; Bénézeth and others, 2007). In the SACROC Unit, Carey and others (2007) previously found a single X-ray diffraction peak of dawsonite in the SACROC core and indicated the possibility of dawsonite precipitation. Therefore, in the 3-D upscaled geocellular model, dawsonite was chosen for the secondary minerals with siderite.

Since no direct measurements of BET-surface areas are available, the specific surface area ($A_m=(A\times\nu\times\rho_m)/(V\times M_w)$) proposed by Knauss and others (2005) was calculated using grain volume (V:[m^3]), grain surface area (A:[m^2]), molar volume (ν:[m^3/mol]), molecular weight (M_w:[g/mol]), and mineral density (ρ_m:[g/m^3]), as detailed in table 5. To calculate V and A, the mineral grains are assumed to be spherical. An average grain radius of 0.00125 m is assumed for all minerals except clay minerals (0.000125 m) such as kaolinite and illite.

The kinetic rate law for the dissolution and precipitation of minerals is from Lasaga (1984) with a temperature-dependent rate constant derived by Arrhenius' law:

$$r_m = \mathrm{sgn}\left(A_m k_{25} \exp\left[-\frac{E_a}{R}\left(\frac{1}{T}-\frac{1}{298.15}\right)\right]\left(1-\frac{Q_m}{K_m}\right)\right) \quad (7)$$

Where, m is the mineral index, r is the dissolution/precipitation rate [mol/m^3s] (positive value indicates precipitation and negative value indicates dissolution), A_m is the reactive surface area [m^2/m^3], k_{25} is the kinetic rate coefficient at 25°C [mol/m^2s], E_a is the activation energy [J/mol], R is the gas constant [8.314 $J/mol\ K$], K_m is the equilibrium constant for mineral reaction, and finally, Q_m is the activity product. As shown in eq 7, the kinetic rate law is limited to describe the growth of secondary minerals in relation to nucleation, preferential growth, and Ostwald ripening, with which only a few studies have been previously concerned (Steefel and van Cappellen, 1990; Ozkan and Ortoleva, 2000). In addition, the kinetic rate constant is often expressed as the sum of three mechanisms such as neutral, acid, and base mechanisms (Lasaga and others, 1994; Palandri and Kharaka, 2004). Among these three mechanisms, only the neutral mechanism is considered here for simplicity. The kinetic rate coefficients and activation energies of different minerals assigned in the 3-D upscaled geocellular model are summarized in table 5. Some kinetic data are taken directly from the scientific literature and others are set to minerals with known kinetic properties.

Thermodynamic parameters, including equilibrium constants, were chosen from the SOLMINEQ.88 and PHREEQC databases (Kharaka and others, 1989; Parkhurst and Appelo, 1999). Particularly, the equilibrium constant of ankerite, which is a solid-solution between siderite and dolomite, varies with its composition. In a natural system, a binary solid-solution, $Ca(Fe_xMg_{1-x})(CO_3)_2$, where $Mg^{2+}\gg Fe^{2+}$ has been observed (Mozley and Hoernle, 1990), but the end-member ankerite, $CaFe(CO_3)_2$, has not (Chai and Navrotsky, 1996). Therefore, the composition of ankerite is assumed to be $CaFe_{0.25}Mg_{0.75}(CO_3)_2$ and its equilibrium constant is calculated from a regular solid-solution approach (Appelo and Postma, 1993) using free energy data from Wood and Garrels (1992). The detailed calculation of ankerite's equilibrium constant is described in Han (ms, 2008).

TABLE 6

Description of primary and secondary species and their initial concentrations

Primary species	Concentration (mol/l)		Secondary species
H^+	3.981E-7 (pH=6.4)		CO_3^{2-}
K^+	3.981E-7	Estimated	NaCl(aq)
Na^+	1.094E0		$NaCO_3^-$
Ca^{2+}	1.314E-1		$NaHCO_3$(aq)
Mg^{2+}	5.700E-2		$CaCO_3$(aq)
SiO_2(aq)	2.345E-3	Estimated	$CaHCO_3^+$
Al^{3+}	2.318E-11	Estimated	$MgCO_3$(aq)
Fe^{2+}	8.850E-4		$MgHCO_3^+$
Cl^-	1.391E0		$Al(OH)_4^-$
HCO_3^-	5.300E-2		$Al(OH)_3$(aq)
SO_4^{2-}	4.050E-2		$Al(OH)_2^+$
			$Al(OH)^{2+}$
			$FeCl_4^{2-}$
			$FeCl^+$
			$Fe(OH)_2$
			$Fe(OH)^+$
			H_4SiO_4(aq)

For the activity coefficient calculation, the B-dot model (Helgeson, 1969) was implemented in this study because this model is relatively easy to incorporate new species and estimate activity coefficients under high temperature conditions. However, the Pitzer model (Pitzer, 1987) can accurately describe the behavior of electrolyte solutions especially at high ionic strength fluid (Monnin, 1989; Lichtner and Felmy, 2003; Zhang and others, 2006), and furthermore, the Pitzer's ion interaction parameters for various aqueous species are becoming more available (Harvie and others, 1984; Felmy and others, 1994; Azaroual and others, 1997; Accornero and Marini, 2009). In CO_2 sequestration processes, the reservoir fluids into which supercritical-phase CO_2 is injected typically have high ionic strengths. Therefore, the application of the Pitzer model can improve the prediction of activity coefficients compared to the B-dot model implemented in this work. Recently, Gaus (2010) discussed the essentials of the Pitzer model in a CO_2 sequestration problem. From the discussion in Gaus (2010), the application of the Pitzer model coupling into reactive transport simulator, TOUGHREACT, is currently ongoing (Zhang and others, 2006), and the development of the complete database for the Pitzer ion interaction parameters is going to be an essential task. Finally, we acquired the initial concentration of brine chemistry (table 6) in the upscaled geocellular model by batch geochemical modeling with the input of average values of brine water chemistry data (table 1) and mineralogy (table 5).

Assignment of CO_2 injection and production wells.—More than 300 wells have been used for CO_2 injection and production over the last 35 years in the SACROC northern platform. Because the sizes of grid elements in the upscaled geocellular model are larger than the distance between individual wells in the actual field, we were forced to lump groups of wells within each grid element. Each was assigned as an inverted 5-spot pattern, and as such we could not assign the actual number of injection and production wells. Consequently, we implemented 23 pumping (*P*) wells and 22 injection (*I*) wells in the 3-D upscaled model (fig. 8D). In addition, both injection and production

wells are partially penetrated with the intervals of 10 to 20 m, approximately 40 m above from the bottom of the model.

We simulated CO_2 injection and production in the field for a 30-year period, from 1972 to 2002. During this field-operation period, a net of about 6.9 million metric tons of CO_2 (6,944,587,674 kg) has been sequestered in the SACROC northern platform (see the discussion in "SOURCES AND SINKS: ACTUAL CO_2 INJECTION AND PRODUCTION HISTORIES"). Nevertheless, in the 3-D upscaled geocellular model, the exact field injection and production history do not match because of issues associated with the scale of the upscaled grid. Rather, only net storage at the end of injection period was matched. In the upscaled model, the CO_2 net storage was about 6.7 million metric tons (6,745,407,000 kg). Consequently, the relative error of CO_2 net storage between the actual field and the model is 2.9 percent.

Results: Spatial distribution of hydrostratigraphic (mobile)- and residual-trapped CO_2.—Figures 10A and 10B respectively show the spatial distribution of supercritical-phase CO_2 and the associated $k_r^{CO_2}$ values, 100 years after CO_2 injection starts (year 2072). Due to the difficulty of showing three-dimensional distributions, two-dimensional cross-sectional views/slices are presented instead. By comparing the spatial distribution between CO_2 saturation (fig. 10A) and associated $k_r^{CO_2}$ values (fig. 10B), it is possible to distinguish the location of free (mobile) CO_2 and residual (immobile) CO_2. By definition, supercritical-phase CO_2 becomes mobile when the $k_r^{CO_2}$ value is greater than zero. In reverse, the supercritical-phase CO_2 becomes immobile, and its $k_r^{CO_2}$ value is equal to zero. In figure 10A, CO_2 saturation is greater than zero within the CO_2 plumes. However, figure 10B shows that although certain grid-blocks have CO_2 saturations greater than zero, they have a zero value for $k_r^{CO_2}$. These grid-blocks indicate where CO_2 is trapped as a residual form.

According to Juanes and others (2006), mobile CO_2 is located at the front of the CO_2 plume, while residual-trapped CO_2 is located at the tail of the CO_2 plume. Similarly, in this simulation, $k_r^{CO_2}$ values were greater than zero at the front of the CO_2 plume, indicating the presence of mobile CO_2. However, $k_r^{CO_2}$ values were zero at the tail of the CO_2 plume although values of CO_2 saturations were not zero, indicating that supercritical-phase CO_2 was stored in a residual form at the tail of the CO_2 plume. Finally, the distribution of aqueous-phase CO_2 imitates the distribution patterns of supercritical-phase CO_2, but with a wider extent (fig. 10C).

Results: Spatial and temporal distribution of aqueous species and minerals.—For most minerals (especially silicate minerals), two hundred years is an insufficient time to reach equilibrium with reservoir fluids. Even after 200 years, all minerals in the simulation results are still dissolving or precipitating. Generally, mineral changes initiate as the dissolution of CO_2 lowers the pH of reservoir brine, which has also been observed in previous laboratory and field experiments (Bowker and Shuler, 1991; Klusman, 2003; Kaszuba and others, 2005; Kharaka and others, 2006). Decreasing pH subsequently induces changes in aqueous concentrations and minerals. In this simulation, initial pH of the reservoir fluid was 6.4 at year 1972 and decreased to approximately 4.5 at year 2072 after 100 years (fig. 11A). The pH does not decrease below 4.5 because the carbonate rock acts as a buffer. Specifically, the simulated pH (fig. 11A) in the brine-only model was decreased more than the observed pH from the SACROC oil field (table 1). Although various processes and uncertainties among model parameters could result in the discrepancy of model predicted pH, we presume that one of the main causes would be the presence of oil in the field.

Calcite, the major mineral in the SACROC Unit, predominantly dissolves during a 200-year simulation. Both anhydrite and dolomite are the major minerals precipitated in this same period. Dawsonite and ankerite are also precipitated but in minor

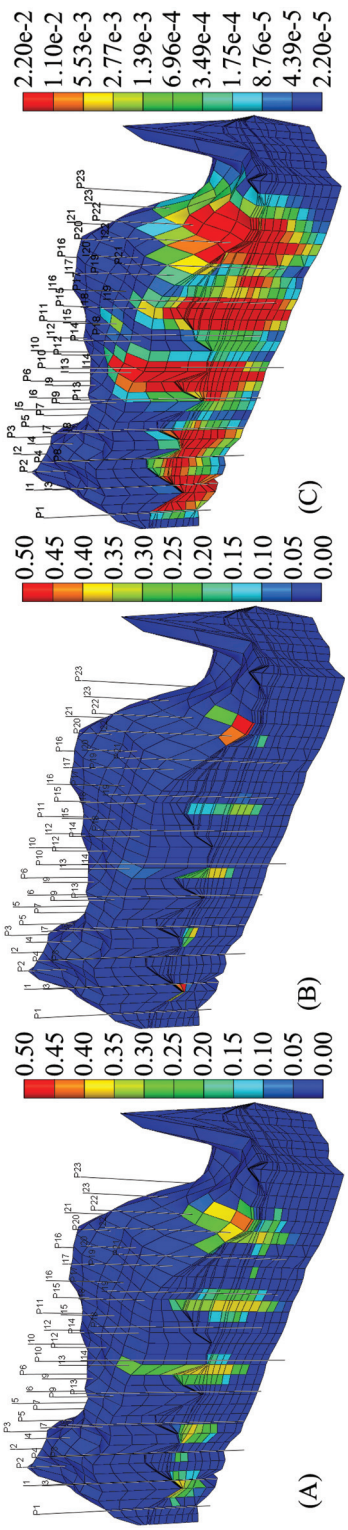

Fig. 10. Two-dimensional cross-section view at year 2072 (100 years after CO_2 injection starts): (A) saturation of supercritical-phase CO_2 with the linear scale, (B) relative permeability ($k_r^{CO_2}$) of supercritical-phase CO_2 with the linear scale, and (C) mole fraction of aqueous-phase CO_2 with the logarithmic scale.

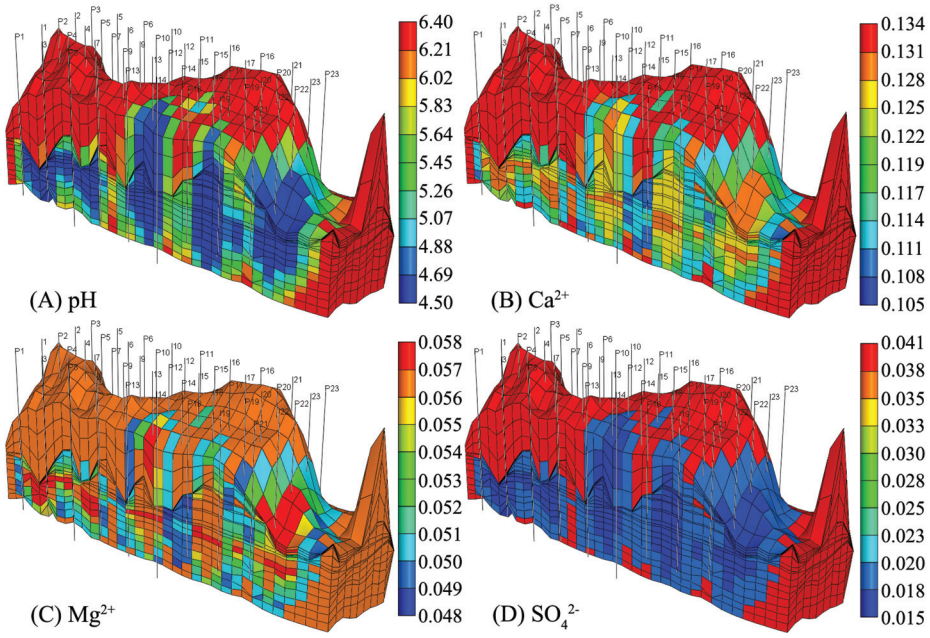

Fig. 11. Two-dimensional cross-section view at year 2072 (100 years after CO_2 injection starts): (A) pH, molalities of (B) Ca^{2+}, (C) Mg^{2+}, and (D) SO_4^{2-}.

amounts. In addition to the carbonate minerals, kaolinite and illite respectively precipitated and dissolved. The associated mineral reactions in this model are:

$$CaSO_4(\text{Anhydrite}) = Ca^{2+} + SO_4^{2-} \quad (8)$$

$$CaCO_3(\text{Calcite}) + H^+ = Ca^{2+} + HCO_3^- \quad (9)$$

$$CaMg(CO_3)_2(\text{Dolomite}) + 2H^+ = Ca^{2+} + Mg^{2+} + 2HCO_3^- \quad (10)$$

$$CaFe_{0.25}Mg_{0.75}CO_3(\text{Ankerite})\ 2H^+ = Ca^{2+} + 0.25Fe^{2+} + 0.75Mg^{2+} + 2HCO_3 \quad (11)$$

$$FeCO_3(\text{Siderite}) + H^+ = Fe^{2+} + HCO_3^- \quad (12)$$

$$NaAl(CO_3)(OH)_2(\text{Dawsonite}) + 3H^+ = Na^+ + Al^{3+} + HCO_3^- + 2H_2O \quad (13)$$

$$Al_2Si_2O_5(OH)_4(\text{Kaolinite}) + 6H^+ = 5H_2O + 2SiO_2(aq) + 2Al^{3+} \quad (14)$$

$$K_{0.6}(Mg_{0.25}Al_{1.8})(Al_{0.5}Si_{3.5})O_{10}(OH)_2(\text{Illite}) + 8H^+ = 0.25Mg^{2+} + 0.6K^+ + 2.3Al^{3+} + 3.5SiO_2 + 5H_2O \quad (15)$$

Mineral precipitation and dissolution patterns are closely related to spatially varying aqueous species. Figure 11B shows the spatial distribution of Ca^{2+} ions. Calcite dissolution (eq 9 and fig. 12A) supplies Ca^{2+} ions to the reservoir brine and triggers the precipitation of dolomite (eq 10 and fig. 12B), anhydrite (eq 8 and fig. 12C), and ankerite (eq 11 and fig. 12D). Especially, CO_2 injection induces the dolomitization process with concurrent calcite dissolution. Previous laboratory studies suggested that elevated temperature, exceeding 60°C, initiates precipitation of dolomite (Usdowski,

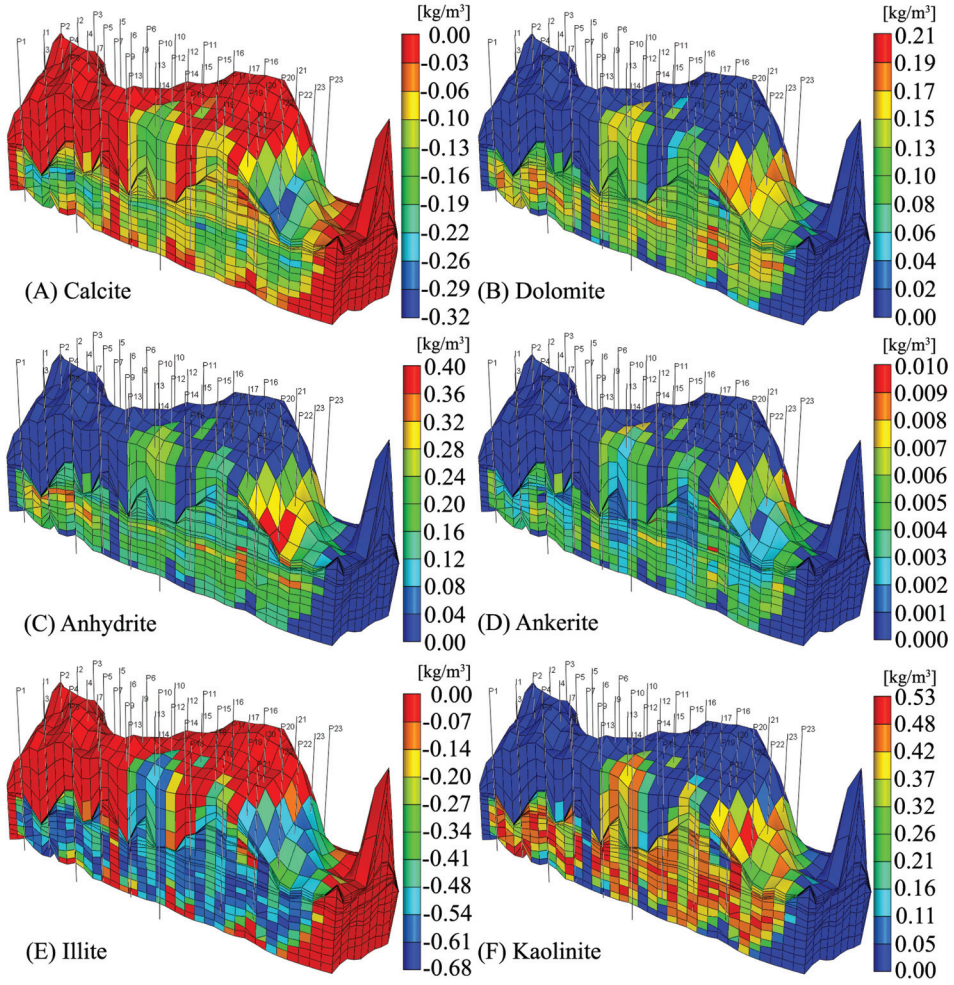

Fig. 12. Two-dimensional cross-section view of minerals (kg/m^3) at year 2072 (100 years after CO_2 injection starts): (A) calcite, (B) dolomite, (C) anhydrite, (D) ankerite, (E) illite, and (F) kaolinite.

1994) although dolomite generally does not precipitate at surface temperature. Similarly, the model predicts that subsurface reservoir temperature is close to 60°C in the SACROC Unit and a high Mg^{2+} concentration in brine fluid initiates dolomite precipitation.

Figure 11C shows the spatial distribution of Mg^{2+} ions, which are consumed during the precipitation of dolomite (fig. 12B) and ankerite (fig. 12D), and concurrently, supplied from the dissolution of illite (fig. 12E). Mg^{2+} concentration in brine fluid was initially 0.057 molality and was depleted to approximately 0.050 molality (fig. 11C) after 100 years (year 2072), suggesting that the Mg^{2+} ion consumption for dolomite and ankerite precipitations is greater than Mg^{2+} ions supply from illite dissolution. In addition to illite, other Mg-bearing aluminosilicates such as montmorillonite and saponite occur naturally. Although these two minerals were not implemented in this simulation, the presence of these minerals in a natural system could affect both Mg^{2+} and Al^{3+} concentration. Finally, calcite dissolution and high SO_4^{2-} concentration in

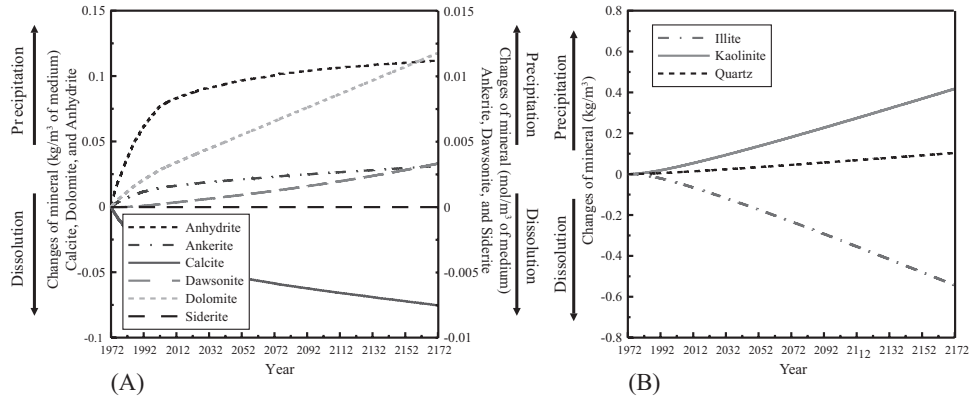

Fig. 13. Temporal evolution of net changes of minerals per the total model volume (kg per m^3): (A) carbonate minerals and (B) silicate and clay minerals.

reservoir brine induces anhydrite precipitation (fig. 12C). Due to anhydrite precipitation, SO_4^{2-} concentration in the brine fluid decreased from an initial 0.04 molality to 0.018 molality after 100 years (fig. 11D).

Reactions involving aluminosilicate minerals have been observed experimentally by Bertier and others (2006). In this SACROC simulation, illite and kaolinite respectively dissolved and precipitated (figs. 12E and 12F). Although kinetic rates of aluminosilicate minerals are slow, the chemical reactions of such aluminosilicate minerals can change the concentration of Al^{3+} ions in brine and cause dawsonite to precipitate (Xu and others, 2004; Hellevang and others, 2005; Audigane and others, 2007). In this simulation, Al^{3+} is supplied from illite dissolution and consumed for the precipitation of kaolinte and dawsonite. Through the simulation period, Al^{3+} ions increases from 10^{-11} to 10^{-7} molality due to the dissolution of illite mineral. Consequently, the change in Al^{3+} ion concentration causes precipitation of a small amount of dawsonite after 100 years. Again, the presence of other aluminosilicate minerals in a natural system could affect this process.

In addition to the spatial distribution of minerals, the temporal evolutions of net changes of minerals per the total model volume (kg per m^3) are predicted during the 200-year simulation period and plotted in figures 13A and 13B. Over a 200 year period, approximately 0.12 kg per m^3 of dolomite, 0.11 kg per m^3 of anhydrite, 0.003 kg per m^3 of ankerite, 0.003 kg per m^3 of dawsonite are precipitated, and about 0.076 kg per m^3 of calcite is dissolved (fig. 13A). In addition to carbonate minerals, 0.43 kg per m^3 of kaolinite, 0.11 kg per m^3 of quartz are precipitated, and about 0.56 kg per m^3 of illite is dissolved (fig. 13B).

The mineral changes of simulated dissolution and precipitation cause changes in porosity. The altered porosity field is shown in figure 14A, indicating the net reduction ($\Delta\phi = \phi_{\text{initial}} - \phi_{\text{current}}$) of porosity due to CO_2 injection. After 100 years, mineral precipitation due to CO_2 sequestration causes the reduction of porosity by approximately 7.5e-5. The corresponding changes of permeability are calculated from the Kozeny-Carman model:

$$\frac{k_{current}}{k_{initial}} = \left(\frac{\phi_{current}}{\phi_{initial}}\right)^3 \left(\frac{1-\phi_{initial}}{1-\phi_{current}}\right)^2 \tag{16}$$

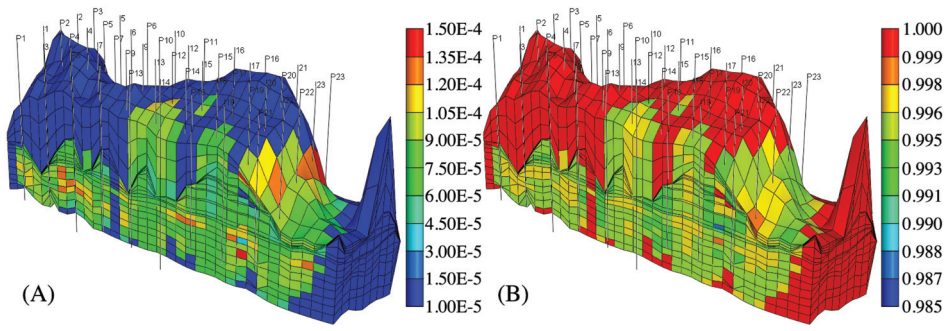

Fig. 14. Changes of porosity ($\Delta\phi = \phi_{initial} - \phi_{current}$) and permeability ($k_{current}/k_{initial}$) at year 2072 (100 years after CO_2 injection starts): (A) porosity and (B) permeability.

where ϕ is the porosity, k is the permeability (m^2). The altered permeability field ($k_{current}/k_{initial}$) is shown in figure 14B. The corresponding permeability reduction was about 0.993.

Results: Quantification of CO_2 trapping mechanisms.—Figure 15A summarizes the CO_2 mass stored in different forms, with CO_2 trapping mechanisms detailed in injection and post-injection periods. During the injection period (1972-2002), 6.7 million metric tons of CO_2 are sequestered into the Cisco and Canyon Groups of the 3-D upscaled geocellular model. In this period, the CO_2 saturation gradually increases near the injection wells. At the same time, the CO_2 plume migrates either vertically or horizontally through preferential flow paths due to the injection-induced pressure. Specifically, the amount of mobile CO_2 increases up to 5.0 million metric tons without increasing immobile CO_2 until the end of the injection period, suggesting that a drainage process [CO_2 (=the non-wetting phase) displaces brine (=the wetting phase)] occurs. In addition, CO_2 injection increases reservoir pressure, leading to the increased CO_2 dissolution in brine. As a result, the mass of solubility-trapped CO_2 sharply increases up to 1.7 million metric tons at the end of the injection period.

After CO_2 injection ends (2002-2172; post injection period), the CO_2 plume starts to migrate upward due to the buoyant force associated with the density contrast between reservoir brine and CO_2. While the CO_2 plume migrates vertically, some CO_2 becomes trapped as a residual form at the tail of the CO_2 plume where imbibition (brine displaces CO_2) occurs. Due to this process, the amount of residual-trapped CO_2 increases dramatically immediately after CO_2 injection stops, and consequently, the amount of mobile CO_2 decreases (fig. 15A). Simulation results suggest that the vertical CO_2 migration after injection stops is the critical factor governing the residual CO_2 trapping mechanism. After 200 years of CO_2 injection, the mass of mobile CO_2 and immobile CO_2 becomes 1.5 million and 2.8 million metric tons, respectively. Finally, the mass of solubility-trapped CO_2 continues to increase to 2.3 million metric tons, but at a slower rate because injection-induced CO_2 partial pressure decreases almost immediately after CO_2 injection ceases. Relatively small amounts (0.17 million metric tons of CO_2) of minerals precipitate after 200 years.

As shown, previous researchers concurred that the most effective short-term storage mechanism is residual CO_2 trapping, and its sensitivity is strongly dependent on S_{gr}^{max} in the Land hysteresis equation shown as eq 6 (Kumar and others, 2005; Juanes and others, 2006; Doughty, 2007). However, until now, only one laboratory dataset (Suekane and others, 2008) predicting S_{gr}^{max} in the supercritical CO_2/brine system has been available. Due to this reason, many researchers rely on one fitting equation developed with data from gas reservoirs (Holtz, 2002). Therefore, we performed

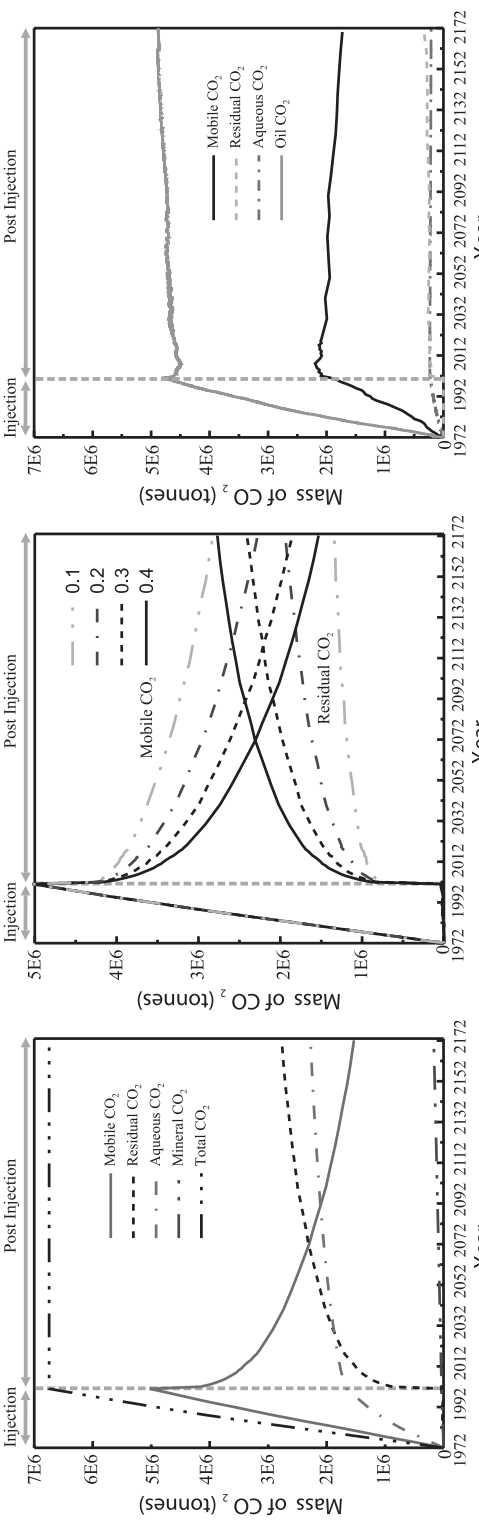

Fig. 15. (A) CO_2 trapping mechanisms in brine-only model as a function of time, (B) sensitivity studies of mobile and residual-trapped CO_2 with S_{gr}^{max} in brine-only model, and (C) CO_2 trapping mechanisms in brine+oil model as a function of time.

TABLE 7

Initial oil composition (Dicharry and others, 1973) in the upscaled geocellular model

Oil Composition	Mol	Molecular Weight
CO_2	0.0032	44.01
N_2	0.0083	28.01
C1(Methane)	0.2865	16.04
C2(Ethane)	0.1129	30.07
C3(Propane)	0.1239	44.10
I-C4(I-Butane)	0.0136	58.12
N-C4(N-Butane)	0.0646	58.12
I-C5(I-Pentane)	0.0198	72.15
N-C5(N-Pentane)	0.0251	72.15
FC6(Hexane)	0.0406	86.00
C7+(Heptanes plus)	0.3015	275.00

sensitivity studies of CO_2 trapping mechanisms with $S_{gr}^{\max}$. Simulation results predicted that the amount of residual-trapped CO_2 increases with larger $S_{gr}^{\max}$ (fig. 15B). For example, residually trapped CO_2 with 0.1 $S_{gr}^{\max}$ was 1.35 million metric tons after 200 years and with 0.4 $S_{gr}^{\max}$ was 2.78 million metric tons. Results suggest that the predicted amount of residually trapped CO_2 can be doubled with the choice of $S_{gr}^{\max}$.

SACROC CO_2 Trapping Model—Oil and Brine

Initial and boundary conditions.—The initial conditions for pressure and temperature distribution and boundary conditions are the same as those described in the previous section "*SACROC CO_2 Trapping Model—Brine Only*". However, the initial condition for fluid saturation is different from that of the brine-only model. The reservoir is assumed to be saturated with both water (0.28) and oil (0.72), following reservoir characterization details provided by Vest (1970). The oil phase is regarded as a mixture of 11 different gas components. The initial oil composition used is from Dicharry and others (1973), summarized in table 7.

Transport input data and well assignment.—Oil densities are calculated from the Peng-Robinson equation of state (Peng and Robinson, 1976) and Oil viscosity is estimated from Jossi and others (1962). CO_2 solubility in oil is predicted from flash calculations, which are decoupled from the transport equation and solved using the Quasi Newton Successive Substitution (Nghiem, 1983). The $k_r^{CO_2}$ curve and its hysteretic effect is the same as those in brine-only model. The k_r^{oil} curve is developed after extrapolating data from the SACROC core measured at 50°C and 1.4 MPa (Rohan and Haggerty, 1996). Finally, the feature of well assignments and performance period were the same as those described in the previous section "*Assignment of CO_2 injection and production wells*".

Results: Quantification of CO_2 trapping mechanisms.—Figure 15C shows simulation results describing the temporal evolution of the CO_2 mass sequestered in the SACROC model saturated with both brine and oil. Specifically, the slope of oil-CO_2 curve is steep during the period between 1972 to 2002. Significant amounts of CO_2 (about 4.5 million metric tons) dissolved into oil during this period. Compared to CO_2 dissolved in oil, only a small amount of CO_2 (about 0.2 million metric tons) dissolves in the brine in the same period. The difference of CO_2 dissolution in both oil and brine is caused

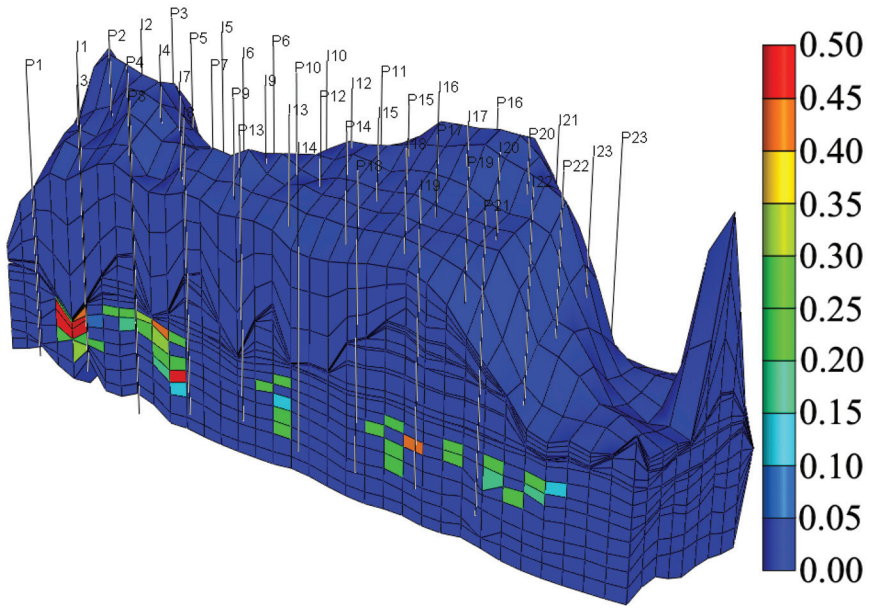

Fig. 16. Two-dimensional cross-section view of saturation of supercritical-phase CO_2 in brine+oil model at year 2072 (100 years after CO_2 injection starts).

by the difference of CO_2 solubility in both fluids and initial fluid saturation. The model predictions show that the approximate CO_2 solubility was respectively 0.010~0.018 mole fraction in brine and 0.3~0.6 mole fraction in oil at this reservoir condition. That is to say, CO_2 solubility in oil was about 30~40 times greater than that in brine. Moreover, oil saturation (0.72) was greater than brine saturation (0.28) in this model indicating that more oil volume is available for CO_2 dissolution. Therefore, the oil-solubility trapping is significantly greater than the brine-solubility trapping in this model. The amount of mobile CO_2 increased up to about 2.1 million metric tons at the end of the injection year (fig. 15C). Similar to the brine-only model, no CO_2 is trapped as a residual form during the injection period (1972-2002). Overall, the dominant CO_2 trapping mechanism is oil trapping, with about 4.5 million metric tons of CO_2 dissolved in the oil during the full 200-year simulation periods. In addition, about 2.1 million metric tons of CO_2 is stored as a mobile form.

In the previous brine-only model, the amount of mobile CO_2 is dramatically decreased and the amount of residual CO_2 is suddenly increased after CO_2 injection stops (fig. 15A). However, in the brine+oil model, the relative amounts of both mobile and residual CO_2 do not change over time (fig. 15C). Further, compared to the amount of residual-trapped CO_2 in the brine-only model, residual-trapped CO_2 in the brine+oil model is significantly less (fig. 15C). To investigate the difference of the amount of residual-trapped CO_2 in both simulations, the saturations of supercritical-phase CO_2 at year 2072 were plotted and compared (figs. 10A and 16). The comparison of CO_2 plume saturation shows that CO_2 migration behavior is distinctively different in both simulations. After 100 years, supercritical-phase CO_2 in the brine-only model migrated vertically and several CO_2 plumes were able to reach the top of the Cisco and Canyon Groups (fig. 10A). The amount of residual-trapped CO_2 increased at the tail of the CO_2 plumes while supercritical-phase CO_2 plumes migrated vertically. However, in the brine+oil model, supercritical-phase CO_2 did not migrate vertically

but stayed near the injection wells with a high CO_2 saturation (fig. 16). In general, supercritical-phase CO_2 in the brine+oil model is stored as a mobile form due to its high CO_2 saturation but does not migrate vertically due to smaller density contrast between oil and supercritical-phase CO_2 and larger CO_2 solubility in oil. Therefore, mobile CO_2 in the brine+oil model behaves like residual-trapped CO_2.

To evaluate the difference of CO_2 vertical migration behavior between brine-only and brine+oil models (figs. 10A and 16), the density of CO_2, brine, and oil phases in this model were compared. Model prediction in brine+oil model shows that the densities of CO_2, oil, and brine are, respectively, about 700~800 kg/m^3, 800 kg/m^3, and 1100 kg/m^3 at these reservoir conditions. Since oil is a dominant fluid (72% saturation), the density contrast between supercritical-phase CO_2 and oil is smaller than about 100 kg/m^3, which is 3~4 times smaller than that between supercritical-phase CO_2 and brine. Since the density contrast between oil and supercritical-phase CO_2 is small, the vertical CO_2 migration is small. (In the simulations of brine+oil model, no CO_2 plume reaches the top of the Cisco and Canyon Groups after 200 years.) Consequently, the amount of residual-trapped CO_2 is not significant (less than 0.3 million metric tons) in this model (fig. 15C). In addition to the contrast of fluid densities, CO_2 mobility is reduced when three phases coexist, for example, injecting CO_2 in a brine+oil reservoir, as opposed to injecting into a reservoir with brine only. In the brine+oil model representing a three-phase environment, the vertical movement of supercritical-phase CO_2 will be relatively retarded. Furthermore, significant CO_2 solubility in the oil phase reduces the volume of supercritical-phase CO_2 in brine+oil model and reduces buoyant force. In summary, the buoyancy-driven force was lower in the brine+oil reservoir model due to less contrast in fluid densities, smaller mobility, and larger CO_2 solubility in the oil phase. Consequently, supercritical-phase CO_2 did not migrate vertically but tended to stay closer to the injection wells.

SUMMARY AND CONCLUSIONS

The main purpose of this research was to predict CO_2 trapping mechanisms in the SACROC northern platform where about 7 million metric tons of CO_2 have been injected for the purpose of enhanced oil recovery from 1972 to 2002. This model was carefully developed with a dataset that includes injection/production history data since 1948 and water chemistry data from both reservoir brine and shallow groundwater. First, a 3-D, high-resolution, geocellular model describing the detailed reservoir structure and heterogeneity was constructed. After the renormalization process for reducing the number of model elements to manageable levels to fit on a single workstation, two models evaluating CO_2 trapping mechanisms in the SACROC northern platform were developed. Initial/boundary conditions, and other parameters in this model were carefully chosen based on the results of data analyses such as groundwater chemistry and CO_2 injection/production history. The first model was designed for simulating CO_2 trapping mechanisms in a reservoir only saturated with brine. The second model was designed for simulating CO_2 trapping mechanisms in a reservoir saturated with both brine and oil. As far as we know, this is the first attempt to compare the fate and distribution of supercritical-phase CO_2 in a reservoir containing both oil and brine versus a reservoir containing brine only. Major conclusions in this work are as follows:

1. Incorporating geologic knowledge, geophysical logs, and seismic surveys provided a foundation for interpreting 3-dimensional subsurface structures. The geocellular model reveals that the Upper Canyon Group is represented as a thick, highly porous zone (fig. 6B) and the Middle/Lower Canyon Group consists of several layered porosity zones separated by low porous carbonate mud.

2. Direct application of the subsurface structure model to develop the flow and transport models is hindered due to the lack of currently available computer resources. The renormalization technique successfully upscaled the model from 9,450,623 to 15,470 elements with a preservation of the variation of heterogeneity (figs. 8A-D).
3. Modeled CO_2 fugacity of reservoir fluids in the Cisco and Canyon Groups was significantly increased during the CO_2 injection period (table 1) but it did not vary in shallow groundwater above the Wolfcamp Shale Formation (table 4), suggesting that the Wolfcamp Shale Formation typically acts as a suitable seal in the SACROC Unit. However, analysis of water chemistry also revealed that a few shallow groundwater samples underwent local contamination with reservoir brine possibly due to the downward recharge of recycled reservoir brine from the surface during enhanced oil recovery or upward leakage of CO_2-saturated brine through the Wolfcamp Shale Formation.
4. CO_2 trapping mechanisms in the brine-only model showed two distinctive periods (fig. 15A). During the injection period (1972~2002), most supercritical-phase CO_2 is stored as mobile phase. After CO_2 injection ceases, the amount of mobile CO_2 dramatically decreases and residual-trapped CO_2 consequently increases. Therefore, during the post injection period (2002~2172), both the residual trapping and solubility trapping mechanisms become dominant. In addition, the amount of residually trapped CO_2 is strongly dependent on the $S_{gr}^{\max}$ in Land Equation (fig. 15B).
5. In the reservoir model with oil (72%) and brine (28%) phases, CO_2 trapping mechanisms do not vary distinctly over time (fig. 15C). The dominant trapping mechanism is oil trapping. Most supercritical-phase CO_2 is stored as a mobile phase near the injection wells and does not migrate; behaving much like residually trapped CO_2. This occurs because of a lower contrast in fluid densities, smaller mobility, and larger CO_2 solubility in oil phase.
6. Mobile CO_2 is located at the front of the CO_2 plume where drainage is dominant (CO_2 displaces water), while residually trapped CO_2 is located at the tail of the CO_2 plume where imbibition is dominant (water displaces CO_2).
7. Injected CO_2 is stored as several different forms of minerals in the brine-only model (figs. 13A and 13B). Calcite (0.076 kg per m^3), the major mineral in the SACROC Unit, predominantly dissolves after a 200-year simulation. Both anhydrite (0.11 kg per m^3) and dolomite (0.12 kg per m^3) are the major minerals precipitated in the same period. Dawsonite (0.003 kg per m^3) and ankerite (0.003 kg per m^3) are also precipitated but in minimal amounts. In addition to the carbonate minerals, kaolinite (0.43 kg per m^3) and illite (0.56 kg per m^3) are precipitated and dissolved, respectively.
8. The induced porosity changes due to mineralization are minor during 100 years. Mineral precipitation due to CO_2 sequestration causes the reduction of porosity by approximately 7.5e-5 after 100 years (fig. 14A). The corresponding permeability reduction was 0.993 (fig. 14B).

The results of CO_2 trapping mechanisms presented here possess some limitations associated with upscaling, including effects of grid-coarsening and averaged ("smoothed") values of porosity and permeability. In the geocellular model, renormalization decreases the number of elements from 9,450,623 to 15,470 as shown in table 3 and, correspondingly, increases the grid size. Through the upscaling procedure, it is clear that the contrast in permeability between adjacent elements becomes smaller (figs. 8A-D), and thus, standard deviation of effective permeability decreases (table 3). Previously, only a few studies evaluated the grid coarsening effects on CO_2 trapping mechanisms and these previous studies only considered grid effects within homoge-

neous models (Solubility trapping by Doughty and Pruess, 2004; Residual CO_2 trapping by Juanes and others, 2006; mineral trapping by Audigane and others, 2007; Yamamoto and Doughty, 2009). All these studies have suggested that the grid coarsening would generate certain errors in predicting CO_2 trapping mechanisms. Although we did not include the study associated with the grid effect here, we investigated the renormalization effect on various 2-dimensional heterogeneous permeability fields and found that the sequential renormalization underestimated residual CO_2 trapping by increasing grid scale and averaging permeability. Therefore, we expected that the residual CO_2 trapping in the presented SACROC model could be underestimated. In future work, we will employ massively parallel computing using the code, PFLOTRAN (Lu and Lichtner, 2007), to predict CO_2 trapping mechanisms in the 3-D geocellular model without the need for upscaling.

Finally, the prediction of spatiotemporal CO_2 trapping mechanisms (mobile CO_2, residual CO_2, dissolved CO_2, and mineral) is one of the daunting problems because (1) the nature of CO_2 trapping is dependent on time and space, (2) individual trapping mechanisms are strongly coupled with each other, and (3) subsurface conditions and properties are altered significantly with CO_2 injection. More importantly, it is difficult to acquire field data from the targeted formations typically below 800 m and monitor their *in-situ* variations. Therefore, previous models predicting CO_2 trapping mechanisms always included certain limitations. In this study, we utilized a specific site with the detailed 3-D geologic frame model, relevant laboratory, and field data to overcome the limitation of previous studies. As a result, this study provides the first successful quantification of all significant CO_2 trapping mechanisms concurrently based on the detailed geologic model. We expect that the processes of model development are intended to serve as an exemplary or template procedure for evaluating the relative roles of different CO_2 trapping mechanisms at other geological storage sites.

Acknowledgments

The authors would like to thank Mike Raines and Renee Robertson at Kinder Morgan Inc. for the useful discussion and CMG Ltd. for allowing us to use their GEM simulator in this research. We also appreciated Dr. Audigane, Dr. Marini, and Dr. Firoozabadi for their thoughtful reviews. This work was part of a Ph.D. dissertation studied at New Mexico Institute of Mining and Technology mentored by various committees including Dr. John L. Wilson, Fred M. Phillips, and Peter S. Mozley and partly supported by the Southwest Regional Partnership CO_2 Project funded by U.S. Department of Energy, under the contract no. DE-FC26-06NT42591.

References

Accornero, M., and Marini, L., 2009, Empirical prediction of the Pitzer's interaction parameters for cationic Al species with both SiO_2(aq) and CO_2(aq): Implications for the geochemical modeling of very saline solutions: Applied Geochemistry, v. 24, p. 747–759, doi:10.1016/j.apgeochem.2009.01.002.

Allen, H. H., and LaRue, C. R., 1957, SACROC Unit operations: Journal of Petroleum Technology, v. 9, p. 21–25, doi:10.2118/829-G.

Allen, H. H., and Thomas, J. B., 1959, Pressure maintenance in SACROC Unit operations January 1, 1959: Journal of Petroleum Technology, v. 11, p. 42–48, doi:10.2118/1259-G.

Allis, R., White, S., Chidsey, T., Gwynn, W., Morgan, C., Adams, M., and Moore, J., 2001, Natural CO_2 reservoirs on the Colorado plateau and southern Rocky Mountains: Candidate for CO_2 sequestration: Washington, D. C., May 14–17, 2001, Proceedings of the First National Conference on Carbon Sequestration, 19 p., DOE-NETL CD DOE/NETL-2001/1144.

Altevogt, A. S., and Celia, M. A., 2004, Numerical modeling of carbon dioxide in unsaturated soils due to deep subsurface leakage: Water Resources Research, v. 40, 9 p., W03509, doi:10.1029/2003WR002848.

André, L., Audigane P., Azaroual M., and Menjoz, A., 2007, Numerical modeling of fluid-rock chemical interactions at the supercritical CO_2-liquid interface during CO_2 injection into a carbonate reservoir, the Dogger aquifer (Paris basin, France): Energy Conversion and Management, v. 48, p. 1782–1797, doi:10.1016/j.enconman.2007.01.006.

André, L., Azaroual, M., and Menjoz, A., 2010, Numerical simulations of the thermal impact of supercritical CO_2 injection on chemical reactivity in a carbonate saline reservoir: Transport in Porous Media, v. 82, p. 247–274, doi:10.1007/s11242-009-9474-2.

Appelo, C. A. J., and Postma, D., 1993, Geochemistry, Groundwater and Pollution: Rotterdam, The Netherlands, Balkema A.A. Publishers, 536 p.

Audigane, P., Gaus, I., Czernichowski-Lauriol, I., Pruess, K., and Xu, T., 2007, Two-dimensional reactive transport modeling of CO_2 injection in a saline aquifer at the Sleipner site, North Sea: American Journal of Science, v. 307, p. 974–1008, doi:10.2475/07.2007.02.

Azaroual, M., Fouillac, C., and Matray, J. M., 1997, Solubility of silica polymorphs in electrolyte solutions, I. Activity coefficient of aqueous silica from 25° to 250°C, Pitzer's parameterisation: Chemical Geology, v. 140, p. 155–165, doi:10.1016/S0009-2541(97)00046-6.

Bachu, S., and Adams, J. J., 2003, Sequestration of CO_2 in geological media in response to climate change: capacity of deep saline aquifers to sequester CO_2 in solution: Energy Conversion and Management, v. 44, p. 3151–3175, doi:10.1016/S0196-8904(03)00101-8.

Bachu, S., Bonijoly, D., Bradshaw, J., Burruss, R., Holloway, S., Christensen, N. P., and Mathiassen, O. M., 2007, CO_2 storage capacity estimation: Methodology and gaps: International Journal of Greenhouse Gas Control, v. 1, p. 430–443, doi:10.1016/S1750-5836(07)00086-2.

Baker, J. C., Bai, G. P., Hamilton, P. J., Golding, S. D., and Keene, J. B., 1995, Continental-scale magmatic carbon dioxide seepage recorded by dawsonite in the Bowen-Gunnedah-Sydney basin system, eastern Australia: Journal of Sedimentary Research, v. A65, p. 522–530.

Bakker, R. J., 2003, Package *FLUIDS* 1. Computer programs for analysis of fluid inclusion data and for modelling bulk fluid properties: Chemical Geology, v. 194, p. 3–23, doi:10.1016/S0009-2541(02)00268-1.

Bando, S., Takemura, F., Nishio, M., Hihara, E., and Akai, M., 2004, Viscosity of aqueous NaCl solutions with dissolved CO_2 at (30 to 60)°C and (10 to 20) MPa: Journal of Chemical and Engineering Data, v. 49, p. 1328–1332, doi:10.1021/je049940f.

Barlet-Gouêdard, V., Rimmelé, G., Goffé, B., and Porcherie, O., 2006, Mitigation strategies for the risk of CO_2 migration through wellbores: Miami, Florida, USA, February 21–23, 2006, Proceedings of the IADC/SPE Drilling Conference.

Bayat, M. G., Pickard, C. D., Benvegnu, A. J., Wingate, T. P., and Larkin, R., 1996, Linking reservoir characteristics and recovery processes at SACROC-controlling wasteful cycling of fluids at SACROC while maximizing reserves: Second Annual Subsurface Fluid Control Symposium and Conference.

Bénézeth, P., Palmer, D. A., Anovitz, L. M., and Horita, J., 2007, Dawsonite synthesis and reevaluation of its thermodynamic properties from solubility measurements: Implications for mineral trapping of CO_2: Geochimica et Cosmochimica Acta, v. 71, p. 4438–4455, doi:10.1016/j.gca.2007.07.003.

Bennion, B., and Bachu, S., 2005, Relative permeability characteristics for supercritical CO_2 displacing water in a variety of potential sequestration zones in the western Canada sedimentary basin: Dallas, Texas, USA, October 9–12, 2005, Proceedings of the 2005 SPE Annual Technical Conference and Exhibition, *SPE 95547* (2005).

——— 2006, The impact of interfacial tension and pore size distribution/capillary pressure character on CO_2 relative permeability at reservoir conditions in CO_2-brine system: SPE/DOE symposium on Improved Oil Recovery, 22–26 April 2006, Tulsa Oklahoma, USA.

Bergenback, R. E., and Terriere, R. T., 1953, Petrography and petrology of Scurry reef, Scurry County, Texas: AAPG Bulletin, v. 37, p. 1014–1029.

Bertier, P., Swennen, R., Laenen, B., Lagrou, D., and Dreesen, R., 2006, Experimental identification of CO_2-water-rock interactions caused by sequestration of CO_2 in Westphalian and Buntsandstein sandstones of the Campine basin (NE-Belgium): Journal of Geochemical Exploration, v. 89, p. 10–14, doi:10.1016/j.gexplo.2005.11.005.

Bethke, C. M., 1996, Geochemical Reaction Modeling: New York, University Press, 397 p.

Bielinski, A., Kopp, A., Schütt, H., and Class, H., 2008, Monitoring of CO_2 plumes during storage in geological formations using temperature signals: Numerical investigation: International Journal of Greenhouse Gas Control, v. 2, p. 319–328, doi:10.1016/j.ijggc.2008.02.008.

Bowker, K. A., and Shuler, P. J., 1991, Carbon dioxide injection and resultant alteration of the Weber Sandstone, Rangely Field, Colorado: AAPG Bulletin, v. 75, p. 1489–1499.

Bradshaw, J., Bachu, S., Bonijoly, D., Burruss, R., Holloway, S., Christensen, N. P., and Mathiassen, O. M., 2007, CO_2 storage capacity estimation: Issues and development of standards: International Journal of Greenhouse Gas Control, v. 1, p. 62–68, doi:10.1016/S1750-5836(07)00027-8.

Brnak, J., Petrich, B., and Konopczynski, M. R., 2006, Application of SmartWell technology to the SACROC CO_2 EOR project: A case study: Tulsa, Oklahoma, USA, April 22–26, 2006, SPE/DOE Symposium on Improved Oil Recovery.

Brummett, W. W., Jr., Emanuel, A. S., and Ronquille, J. D., 1976, Reservoir description by simulation at SACROC—A case history: Journal of Petroleum Technology, v. 28, p. 1241–1255.

Burnside, R. J., 1959, Geology of part of Horseshoe Atoll in Borden and Howard Counties, Texas: Geological Survey Professional Paper 315-B, p. 21–35.

Busch, A., Alles, S., Gensterblum, Y., Prinz, D., Dewhurst, D. N., Raven, M. D., Stanjek, H., and Krooss, B. M., 2008, Carbon dioxide storage potential of shales: International Journal of Greenhouse Gas Control, v. 2, p. 297–308, doi:10.1016/j.ijggc.2008.03.003.

Carey, J. W., Wigand, M., Chipera, S. J., WoldeGabriel, G., Pawar, R., Lichtner, P. C., Wehner, S. C., Raines, M. A., and Guthrie, G. D., Jr., 2007, Analysis and performance of oil well cement with 30 years of CO_2 exposure from the SACROC unit, west Texas, USA: International Journal of Greenhouse Gas Control, v. 1, p. 75–85, doi:10.1016/S1750-5836(06)00004-1.

Chai, L., and Navrotsky, A., 1996, Synthesis, characterization, and energetics of solid solution along the

dolomite-ankerite join, and implications for the stability of ordered $CaFe(CO_3)_2$: American Mineralogist, v. 81, p. 1141–1147.
Chiquet, P., Daridon, J.-L., Broseta, D., and Thibeau, S., 2007, CO_2/water interfacial tensions under pressure and temperature conditions of CO_2 geological storage: Energy Conversion and Management, v. 48, p. 736–744, doi:10.1016/j.enconman.2006.09.011.
Computer Modeling Group, 2008, User's guide GEM, Advanced compositional reservoir simulator (version 2008): Computer Modeling Group Ltd., 954 p.
Cortis, A., Oldenburg, C. M., and Benson, S. M., 2008, The role of optimality in characterizing CO_2 seepage from geologic carbon sequestration sites: International Journal of Greenhouse Gas Control, v. 2, p. 640–652, doi:10.1016/j.ijggc.2008.04.008.
Dicharry, R. M., Perryman, T. L., and Ronquille, J. D., 1973, Evaluation and design of a CO_2 miscible flood project—SACROC Unit, Kelly-Snyder field: Journal of Petroleum Technology, v. 25, p. 1309–1318, doi:10.2118/4083-PA.
Dilmore, R. M., Allen, D. E., Jones, J. R. M., Hedges, S. W., and Soong, Y., 2008, Sequestration of dissolved CO_2 in the Oriskany Formation: Environmental Science and Technology, v. 42, p. 2760–2766, doi: 10.1021/es702229f.
Dixon, B. P., and Newton, L. E., Jr., 1965, Reinjection of large volumes of produced water in secondary operations: Journal of Petroleum Technology, v. 17, p. 781–789, doi:10.2118/1147-PA.
Doughty, C., 2007, Modeling geologic storage of carbon dioxide: Comparison of non-hystereric and hysteretic characteristic curves: Energy Conversion and Management, v. 48, p. 1768–1781, doi:10.1016/j.enconman.2007.01.022.
Doughty, C., and Pruess, K., 2004, Modeling supercritical carbon dioxide injection in heterogeneous porous media: Vadose Zone Journal, v. 3, p. 837–847, doi:10.2113/3.3.837.
Duan, Z., and Sun, R., 2003, An improved model calculating CO_2 solubility in pure water and aqueous NaCl solutions from 273 to 533 K and from 0 to 2000 bar: Chemical Geology, v. 193, p. 257–271, doi:10.1016/S0009-2541(02)00263-2.
Duan, Z., Sun, R., Zhu, C., and Chou, I.-M., 2006, An improved model for the calculation of CO_2 solubility in aqueous solutions containing Na^+, K^+, Ca^{2+}, Mg^{2+}, Cl^-, and SO_4^{2-}: Marine Chemistry, v. 98, p. 131–139, doi:10.1016/j.marchem.2005.09.001.
Duan, Z., Hu, J., Li, D., and Mao, S., 2008, Densities of the CO_2-H_2O and CO_2-H_2O-NaCl systems up to 647 K and 100 MPa: Energy and Fuels, v. 22, p. 1666–1674, doi:10.1021/ef700666b.
Dubessy, J., Tarantola, A., and Sterpenich, J., 2005, Modelling of liquid-vapor equilibria in the H_2O-CO_2-NaCl and H_2O-H_2S-NaCl systems to 270°C: Oil and Gas Science and Technology, v. 60, p. 339–355, doi:10.2516/ogst:2005021.
Dumore, J. M., and Schols, R. S., 1974, Drainage capillary-pressure functions and the influence of connate water: Society of Petroleum Engineers Journal, v. 14, p. 437–444, doi:10.2118/4096-PA.
Emberley, S., Hutcheon, I., Shevalier, M., Durocher, K., Gunter, W. D., and Perkins, E. H., 2004, Geochemical monitoring of fluid-rock interaction and CO_2 storage at the Weyburn CO_2-injection enhanced oil recovery site, Saskatchewan, Canada: Energy, v. 29, p. 1393–1401, doi:10.1016/j.energy.2004.03.073.
Ennis-King, J., and Paterson, L., 2005, Role of convective mixing in the long-term storage of carbon dioxide in deep saline formations: Society of Petroleum Engineers Journal, v. 10, p. 349–356, doi: 10.2118/84344-PA.
——— 2007, Coupling of geochemical reactions and convective mixing in the long-term geological storage of carbon dioxide: International Journal of Greenhouse Gas Control, v. 1, p. 86–93, doi:10.1016/S1750-5836(07)00034-5.
Fairbridge, R. W., 1950, Recent and Pleistocene coral reefs of Australia: The Journal of Geology, v. 58, n. 4, p. 330–401, doi:10.1086/625751.
Farajzadeh, R., Salimi, H., Zitha, P. L. J., and Bruining, H., 2007, Numerical simulation of density-driven natural convection in porous media with application for CO_2 injection projects: International Journal of Heat and Mass Transfer, v. 50, p. 5054–5064, doi:10.1016/j.ijheatmasstransfer.2007.08.019.
Felmy, A. R., Rustad, J. R., Mason, M. J., and de la Bretonne, R., 1994, A chemical model for the major electrolyte components of the Hanford waste tanks: the binary electrolytes in the systems: Na-NO_3-NO_2-SO_4-CO_3-F-PO_4-OH-$Al(OH)_4$-H_2O: Richland, Washington, Pacific Northwest National Laboratory, PNNL Technical Report TWRS-PP-94-090.
Flett, M., Gurton, R., and Weir, G., 2007, Heterogeneous saline formations for carbon dioxide disposal: Impact of varying heterogeneity on containment and trapping: Journal of Petroleum Science and Engineering, v. 57, p. 106–118, doi:10.1016/j.petrol.2006.08.016.
Fleury, M., and Deschamps, H., 2008, Electrical conductivity and viscosity of aqueous NaCl solutions with dissolved CO_2: Journal of Chemical and Engineering Data, v. 53, p. 2505–2509, doi:10.1021/je8002628.
Fuller, R. C., Prevost, J. H., and Piri, M., 2006, Three-phase equilibrium and partitioning calculations for CO_2 sequestration in saline aquifers: Journal of Geophysical Research, v. 111, B06207, doi:10.1029/2005JB003618, doi:10.1029/2005JB003618.
Gale, J., 2004, Geological storage of CO_2: What do we know, where are the gaps and what more needs to be done?: Energy, v. 29, p. 1329–1338, doi:10.1016/j.energy.2004.03.068.
Gasperikova, E., and Hoversten, G. M., 2006, A feasibility study of nonseismic geophysical methods for monitoring geologic CO_2 sequestration: The Leading Edge, v. 25, p. 1282–1288, doi:10.1190/1.2360621.
Gaus, I., 2010, Role and impact of CO_2-rock interactions during CO_2 storage in sedimentary rocks: International Journal of Greenhouse Gas Control, v. 4, p. 73–89, doi:10.1016/j.ijggc.2009.09.015.
Gaus, I., Azaroual, M., and Czernichowski-Lauriol, I., 2005, Reactive transport modelling of the impact of

CO_2 injection on the clayey cap rock at Sleipner (North Sea): Chemical Geology, v. 217, p. 319–337, doi:10.1016/j.chemgeo.2004.12.016.
Gautier, Y., and Noetinger, B., 1997, Preferential flow-paths detection for heterogeneous reservoirs using a new renormalization technique: Transport in Porous Media, v. 26, p. 1–23, doi:10.1023/A:1006515616347.
Gerling, C. R., 1983, McElmo Dome Leadville carbon dioxide field, Colorado, *in* Fassett, J. E., editor, Oil and Gas Fields of the Four Corners Area: Four Corners Geological Survey, v. 3, p. 735–739.
Gherardi, F., Xu, T., and Pruess, K., 2007, Numerical modeling of self-limiting and self-enhancing caprock alteration induced by CO_2 storage in a depleted gas reservoir: Chemical Geology, v. 244, p. 103–129, doi:10.1016/j.chemgeo.2007.06.009.
Giorgis, T., Carpita, M., and Battistelli, A., 2007, 2D modeling of salt precipitation during the injection of dry CO_2 in a depleted gas reservoir: Energy Conversion and Management, v. 48, p. 1816–1826, doi:10.1016/j.enconman.2007.01.012.
Han, W. S., ms, 2008, Evaluation of CO_2 Trapping Mechanisms at the SACROC Northern Platform: Site of 35 Years of CO_2 Injection: Socorro, New Mexico, New Mexico Institute of Mining and Technology, Ph.D. thesis, 465 p.
Han, W. S., Lee, S.-Y., Lu, C., and McPherson, B. J., 2010a, Effects of permeability on CO_2 trapping mechanisms and buoyancy-driven CO_2 migration in saline formations: Water Resources Research, doi:10.1029/2009WR007850.
Han, W. S., Stillman, G. A., Lu, M., Lu, C., McPherson, B. J., and Park, E., 2010b, Evaluation of potential non-isothermal processes and heat transport during CO_2 sequestration: Journal of Geophysical Research, doi:10.1029/2009JB006745.
Harvey, A. H., 1996, Semiempirical correlation for Henry's constants over large temperature ranges: AIChE Journal, v. 42, p. 1491–1494, doi:10.1002/aic.690420531.
Harvie, C. E., Møller, N., and Weare, J. H., 1984, The prediction of mineral solubilities in natural waters: The Na-K-Mg-Ca-H-Cl-SO_4-OH-HCO_3-CO_3-CO_2-H_2O system to high ionic strengths at 25°C: Geochimica et Cosmochimica Acta, v. 48, p. 723–751, doi:10.1016/0016-7037(84)90098-X.
Hawkins, J. T., Benvegnu, A. J., Wingate, T. P., McKamie, J. D., Pickard, C. D., and Altum, J. T., 1996, SACROC Unit CO_2 flood: Multidisciplinary team improves reservoir management and decreases operating costs: SPE Reservoir Engineering, v. 11, p. 141–148, doi:10.2118/35359-PA.
Helgeson, H. C., 1969, Thermodynamics of hydrothermal systems at elevated temperatures and pressures: American Journal of Science, v. 267, p. 729–804.
Hellevang, H., Aagaard, P., Oelkers, E. H., and Kvamme, B., 2005, Can Dawsonite permanently trap CO_2?: Environmental Science and Technology, v. 39, p. 8281–8287, doi:10.1021/es0504791.
Hinrichsen, E. L., Aharony, A., Feder, J., Hansen, A., Jøssang, T., and Hardy, H. H., 1993, A fast algorithm for estimating large-scale permeabilities of correlated anisotropic media: Transport in Porous Media, v. 12, p. 55–72, doi: 10.1007/BF00616362.
Holloway, S., 2005, Underground sequestration of carbon dioxide—a viable greenhouse gas mitigation option: Energy, v. 30, p. 2318–2333, doi:10.1016/j.energy.2003.10.023.
Holtz, M. H., 2002, Residual gas saturation to aquifer flux: A calculation method for 3-D computer reservoir model construction: Calgary, Alberta, Canada, 30 April–2 May 2002, SPE Gas Technology Symposium, SPE 75502.
Hu, J., Duan, Z., Zhu, C., and Chou, I.-M., 2007, *PVTx* properties of the CO_2-H_2O and CO_2-H_2O-NaCl systems below 647 K: Assessment of experimental data and thermodynamic models: Chemical Geology, v. 238, p. 249–267, doi:10.1016/j.chemgeo.2006.11.011.
Ide, S. T., Jessen, K., and Orr, F. M., Jr., 2007, Storage of CO_2 in saline aquifer: Effects of gravity, viscous, capillary forces on amount and timing of trapping: International Journal of Greenhouse Gas Control, v. 1, p. 481–491, doi:10.1016/S1750-5836(07)00091-6.
IEA Greenhouse Gas R&D Programme, 2001, Putting Carbon Back into the Ground: IEA Greenhouse Gas R&D Programme, 28 p.
Intergovernmental Panel on Climate Change, 2005, Carbon Dioxide Capture and Storage: United Kingdom, Cambridge University Press, 431 p.
Jennings, J. W., Jr., and Lucia, F. J., 2003, Predicting permeability from well logs in carbonates with a link to geology for interwell permeability mapping: SPE Reservoir Evaluation and Engineering, v. 6, p. 215–225, doi:10.2118/84942-PA.
Jossi, J. A., Stiel, L. I., and Thodos, G., 1962, The viscosity of pure substances in the dense gaseous and liquid phase: AIChe Journal, v. 8, p. 59–63, doi:10.1002/aic.690080116.
Juanes, R., Spiteri, E. J., Orr, F. M., Jr., and Blunt, M. J., 2006, Impact of relative permeability hysteresis on geological CO_2 storage: Water Resources Research, v. 42, W12418, doi:10.1029/2005WR004806, doi:10.1029/2005WR004806.
Kane, A. V., 1979, Performance review of a large-scale CO2-WAG enhanced recovery project, SACROC Unit Kelly-Snyder field: Journal of Petroleum Technology, v. 31, p. 217–231, doi:10.2118/7091-PA.
Kaszuba, J. P., Janecky, D. R., and Snow, M. G., 2005, Experimental evaluation of mixed fluid reactions between supercritical carbon dioxide and NaCl brine: Relevance to the integrity of a geologic carbon repository: Chemical Geology, v. 217, p. 277–293, doi:10.1016/j.chemgeo.2004.12.014.
Kestin, J., Khalifa, H. E., and Correia, R. J., 1981, Tables of the dynamic and kinematic viscosity of aqueous NaCl solutions in the temperature range 20–150°C and the pressure range 0.1–35 MPa: Journal of Physical and Chemical Reference Data, v. 10, p. 71–87, doi:10.1063/1.555641.
Kharaka, Y. K., Gunter, W. D., Aggarwal, P. K., Perkins, E., and Debraal, J. D., 1989, SOLMINEQ.88: A computer program for geochemical modeling of water-rock reactions: USGS Water-Resources Investigations Report 88-4227.
Kharaka, Y. K., Cole, D. R., Thordsen, J. J., Kakouros, E., and Nance, H. S., 2006, Gas-water-rock interactions

in sedimentary basins: CO_2 sequestration in the Frio Formation, Texas, USA: Journal of Geochemical Exploration, v. 89, p. 183–186, doi:10.1016/j.gexplo.2005.11.077.
King, P. R., 1989, The use of renormalization for calculating effective permeability: Transport in Porous Media, v. 4, p. 37–58, doi:10.1007/BF00134741.
——— 1996, Upscaling permeability: Error analysis for renormalization: Transport in Porous Media, v. 23, p. 337–354, doi:10.1007/BF00167102.
Klusman, R. W., 2003, A geochemical perspective and assessment of leakage potential for a mature carbon dioxide-enhanced oil recovery project and as a prototype for carbon dioxide sequestration; Rangely field, Colorado: AAPG Bulletin, v. 87, p. 1485–1507, doi:10.1306/04220302032.
Knauss, K. G., Johnson, J. W., and Steefel, C. I., 2005, Evaluation of the impact of CO_2, co-contaminant gas, aqueous fluid and reservoir rock interactions on the geologic sequestration of CO_2: Chemical. Geology, v. 217, p. 339–350, doi:10.1016/j.chemgeo.2004.12.017.
Kopp, A., Class, H., and Helmig, R., 2009, Investigations on CO_2 storage capacity in saline aquifers—Part 2: Estimation of storage capacity coefficients: International Journal of Greenhouse Gas Control, v. 3, p. 277–287, doi:10.1016/j.ijggc.2008.10.001.
Kumar, A., Ozah, R. C., Noh, M., Pope, G. A., Bryant, S. L., Sepehrnoori, K., and Lake, L. W., 2005, Reservoir simulation of CO_2 storage in deep saline aquifers: Society of Petroleum Engineers Journal, v. 10, p. 336–348.
Land, C. S., 1968, Calculation of imbibition relative permeability for two- and three-phase flow from rock properties: Society of Petroleum Engineers Journal, v. 8, p. 149–156, doi:10.2118/1942-PA.
Langston, M. V., Hoadley, S. F., and Young, D. N., 1988, Definitive CO_2 flooding response in the SACROC Unit: Tulsa, Oklahoma, USA, 16–21 April, 1988, SPE Enhanced Oil Recovery Symposium, doi: 10.2118/17321-MS.
Lasaga, A. C., 1984, Chemical kinetics of water-rock interactions: Journal of Geophysical Research, v. 89, B6, p. 4009–4025, doi:10.1029/JB089iB06p04009.
Lasaga, A. C., Soler, J. M., Ganor, J., Burch, T. E., and Nagy, K. L., 1994, Chemical weathering rate laws and global geochemical cycles: Geochimica et Cosmochimica Acta, v. 58, p. 2361–2386, doi:10.1016/0016-7037(94)90016-7.
Leverett, M. C., 1941, Capillary behavior in porous solids: Transactions of the American Institute of Mining, Metallurgical, and Petroleum Engineers, v. 142, p. 152–169.
Lewicki, J. L., Hilley, G. E., and Oldenburg, C. M., 2005, An improved strategy to detect CO_2 leakage for verification of geologic carbon sequestration: Geophysical Research Letters, v. 32, L19403, doi:10.1029/2005GL024281, doi:10.1029/2005GL024281.
Li, Y.-K., and Nghiem, L. X., 1986, Phase equilibria of oil, gas, and water/brine mixtures from a cubic equation of state and Henry's Law: Canadian Journal of Chemical Engineering, v. 64, p. 486–496, doi:10.1002/cjce.5450640319.
Lichtner, P. C., and Felmy, A. R., 2003, Estimation of Hanford SX tank waste compositions from historically derived inventories: Computers and Geosciences, v. 29, p. 371–383, doi:10.1016/S0098-3004(03)00012-8.
Litynski, J. T., Plasynski, S., McIlvried, H. G., Mahoney, C., and Srivastava, R. D., 2008, The United States Department of Energy's Regional Carbon Sequestration Partnerships Program validation phase: Environment International, v. 34, p. 127–138, doi:10.1016/j.envint.2007.07.005.
Lu, C., and Lichtner, P. C., 2007, High resolution numerical investigation on the effect of convective instability on long term CO_2 storage in saline aquifers: Journal of Physics: Conference Series, v. 78, 012042, doi:10.1088/1742-6596/78/1/012042.
Lu, J., Wilkinson, M., Haszeldine, R. S., and Fallick, A. E., 2009, Long-term performance of a mudrock seal in natural CO_2 storage: Geology, v. 37, p. 35–38, doi:10.1130/G25412A.1.
Lu, M., and Connell, L. D., 2008, Non-isothermal flow of carbon dioxide in injection wells during geologic storage: International Journal of Greenhouse Gas Control, v. 2, p. 248–258, doi:10.1016/S1750-5836(07)00114-4.
Lucia, F. J., 1995, Rock-fabric/petrophysical classification of carbonate pore space for reservoir characterization: AAPG Bulletin, v. 79, p. 1275–1300.
——— 1999, Carbonate Reservoir Characterization: Berlin, Springer-Verlag, 226 p.
Lucia, F. J., and Kerans, C., 2004, Permeability estimation using porosity logs and rock fabric stratigraphy: an example from the SACROC (Pennsylvanian) field, Scurry County, Texas, *in* Trentham R., editor, Banking on the Permian Basin: Plays, Field Studies, and Techniques: West Texas Geological Society Publication 04-112, p. 271–274.
Malick, K. M., ms, 1995, Boundary effects in the successive upscaling of absolute permeabilities: Palo Alto, California, Stanford University, M.S. thesis.
McPherson, B. J. O. L., Han, W. S., and Cole, B. S., 2008, Two equations of state assembled for basin analysis of multiphase CO_2 flow and in deep sedimentary basin conditions: Computers and Geoscience, v. 34, p. 427–444, doi:10.1016/j.cageo.2007.05.017.
Mito, S., Xue, Z., and Ohsumi, T., 2008, Case study of geochemical reactions at the Nagaoka CO_2 injection site, Japan: International Journal of Greenhouse Gas Control, v. 2, p. 309–318, doi:10.1016/j.ijggc.2008.04.007.
Monnin, C., 1989, An ion-interaction model for the volumetric properties of natural waters: Density of the solution and partial molal volumes of electrolytes to high concentrations at 25°C: Geochimica et Cosmochimica Acta, v. 53, p. 1177–1188, doi:10.1016/0016-7037(89)90055-0.
Moore, J., Adams, M., Allis, R., Lutz, S., and Rauzi, S., 2005, Mineralogical and geochemical consequences of the long-term presence of CO_2 in natural reservoirs: An example from the Springerville-St. Johns field, Arizona, and New Mexico, U.S.A: Chemical Geology, v. 217, p. 365–385, doi:10.1016/j.chemgeo.2004.12.019.
Mozley, P. S., and Hoernle, K., 1990, Geochemistry of carbonate cements in the Sag River and Shublik

Formations (Triassic/Jurassic), North Slope, Alaska: implications for the geochemical evolution of formation waters: Sedimentology, v. 37, p. 817–836, doi:10.1111/j.1365-3091.1990.tb01827.x.
Myers, D. A., Stafford, P. T., and Burnside, R. J., 1956, Geology of the late Paleozoic Horseshoe Atoll in west Texas: Bureau of Economic Geology Publication, n. 5607, 113 p.
Nagy, K. L., 1995, Dissolution and precipitation kinetics of sheet silicates, *in* White A. F., and Brantley S. L., editors, Chemical Weathering Rates of Silicate Minerals: Reviews in Mineralogy and Geochemistry, v. 31, p. 173–233.
National Energy Technology Laboratory, 2005, Regional Carbon Sequestration Partnerships Phase I accomplishments: United States Department of Energy, Office of Fossil Energy, National Energy Technology Laboratory, 15 p.
Newell, D. L., Kaszuba, J. P., Viswanathan, H. S., Pawar, R. J., and Carpenter, T., 2008, Significance of carbonate buffers in natural waters reacting with supercritical CO_2: Implications for monitoring, measuring, and verification (MMV) of geologic carbon sequestration: Geophysical Research Letters, v. 35, L23403, doi:10.1029/2008GL035615, doi:10.1029/2008GL035615.
Nghiem, L. X., 1983, A new approach to quasi-Newton methods with application to compositional modeling: San Francisco, California, USA, 15–18 November, SPE Reservoir Simulation Symposium, doi: 10.2118/12242-MS.
Nghiem, L. X., Sammon, P., Grabenstetter, J., and Ohkuma, H., 2004, Modeling CO_2 storage in aquifers with a fully-coupled geochemical EOS compositional simulator: Tulsa, Oklahoma, USA, 17–21 April 2004, SPE/DOE 14th Symposium on Improved Oil Recovery.
Nordbotten, J. M., Celia, M. A., Bachu, S., and Dahle, H. K., 2005, Semianalytical solution for CO_2 leakage through an abandoned well: Environmental Science and Technology, v. 39, p. 602–611, doi:10.1021/es035338i.
Núñez-López, V., Holtz, M. H., Wood, D. J., Ambrose, W. A., and Hovorka, S. D., 2008, Quick-look assessments to identify optimal CO_2 EOR storage sites: Environmental Geology, v. 54, p. 1695–1706, doi:10.1007/s00254-007-0944-y.
Oldenburg, C. M., and Lewicki, J. L., 2006, On leakage and seepage of CO_2 from geologic storage sites into surface water: Environmental Geology, v. 50, p. 691–705, doi:10.1007/s00254-006-0242-0.
Orr, F. M., Jr., 2004, Storage of carbon dioxide in geologic formations: Journal of Petroleum Technology, v. 56, p. 90–97, doi:10.2118/88842-MS.
Ozkan, G., and Ortoleva, P., 2000, A mesoscopic model of nucleation and Ostwald ripening/stepping: Application to the silica polymorph system: Journal of Chemical Physics, v. 112, p. 10510–10525, doi:10.1063/1.481685.
Palandri, J., and Kharaka, Y. K., 2004, A compilation of rate parameters of water-mineral interaction kinetics for application to geochemical modeling: US Geological Survey Open File Report 2004–1068, 64 p.
Parkhurst, D. L., and Appelo, C. A. J., 1999, User's guide to PHREEQC (version 2)—A computer program for speciation, batch-reaction, one-dimensional transport, and inverse geochemical calculation: U.S. Geological Survey Water-Resources Investigations Report 99–4259, 312 p.
Parry, W. T., Forster, C. B., Evans, J. P., Bowen, B. B., and Chan, M. A., 2007, Geochemistry of CO_2 sequestration in the Jurassic Navajo sandstone, Colorado Plateau, Utah: Environmental Geosciences, v. 14, p. 91–109, doi:10.1306/eg.07120606004.
Peng, D. Y., and Robinson, D. B., 1976, A new two-constant equation of state: Industrial and Engineering Chemistry Fundamentals, v. 15, p. 59–64, doi:10.1021/i160057a011.
Pitzer, K. S., 1987, A thermodynamic model for aqueous solutions of liquid-like density, *in* Carmichael, I. S. E., and Eugster, H. P., editors, Thermodynamic Modeling of Geological Materials: Minerals Fluids and Melts: Reviews in Mineralogy, v. 17, p. 97–142.
Plug, W.-J., and Bruining, J., 2007, Capillary pressure for the sand-CO_2-water system under various pressure conditions. Application to CO_2 sequestration: Advances in Water Resources, v. 30, p. 2339–2353, doi:10.1016/j.advwatres.2007.05.010.
Portier, S., and Rochelle, C., 2005, Modelling CO_2 solubility in pure water and NaCl-type waters from 0 to 300°C and from 1 to 300 bar application to the Utsira formation at Sleipner: Chemical Geology, v. 217, p. 187–199, doi:10.1016/j.chemgeo.2004.12.007.
Pruess, K., 2005, Numerical studies of fluid leakage from a geologic disposal reservoir for CO_2 show self-limiting feedback between fluid flow and heat transfer: Geophysical Research Letters, v. 32, L14404, doi:10.1029/2005GL023250.
——— 2008, Leakage of CO_2 from geologic storage: Role of secondary accumulation at shallow depth: International Journal of Greenhouse Gas Control, v. 2, p. 37–46, doi:10.1016/S1750-5836(07)00095-3.
Pruess, K., and Müller, N., 2009, Formation dry-out from CO_2 injection into saline aquifers: 1. Effects of solids precipitation and their mitigation: Water Resources Research, v. 45, W03402, doi:10.1029/2008WR007101.
Qi, R., LaForce, T. C., and Blunt, M. J., 2009, Design of carbon dioxide storage in aquifers: International Journal of Greenhouse Gas control, v. 3, p. 195–205, doi:10.1016/j.ijggc.2008.08.004.
Raines, M., 2005, Kelly-Snyder (Cisco-Canyon) Fields/SACROC unit: Oil and Gas fields in West Texas VIII: West Texas Geological Society Publication 05-114, p. 69–78.
Ranies, M. A., Dobitz, J. K., and Wehner, S. C., 2001, A review of the Pennsylvanian SACROC Unit, *in* Viveros, J. J., and Ingram, S. M., editors, The Permian Basin: Microns to Satellites, Looking for Oil and Gas at All Scales: West Texas Geological Society Publication 01-110, p. 67–74.
Reid, A. M., and Reid, S. A. T., 1991, The Cogdell field study, Kent and Scurry counties, Texas: A post-mortem, *in* Candelaria, M., editor, The Permian Basin Plays: Tomorrow's Technology Today: West Texas Geological Society Publication 91-89, p. 39–66.
Renard, P., and de Marsily, G., 1997, Calculating equivalent permeability: a review: Advances in Water Resources, v. 20, p. 253–278, doi:10.1016/S0309-1708(96)00050-4.

Renard, P., Le Loc'h, G., Ledoux, E., de Marsily, G., and Mackay, R., 2000, A fast algorithm for the estimation of the equivalent hydraulic conductivity of heterogeneous media: Water Resources Research, v. 36, p. 3576–3580, doi:10.1029/2000WR900203.

Rohan, J. A., and Haggerty, D., 1996, Carbonate species core analysis study for Pennzoil exploration and production company: Elevated temperature centrifuge study: Technical Report, Westport Technology Center, IIT Research Institute.

Rowe, A. M., Jr., and Chou, J. C. S., 1970, Pressure-volume-temperature-concentration relation of aqueous sodium chloride solutions: Journal of Chemical and Engineering Data, v. 15, p. 61–66, doi:10.1021/je60044a016.

Saadatpoor, E., Bryant, S. L., and Sepehrnoori, K., 2010, New trapping mechanism in carbon sequestration: Transport in Porous Media, v. 82, p. 3–17, doi:10.1007/s11242-009-9446-6.

Saripalli, P., Amonette, J., Rutz, F., and Gupta, N., 2006, Design of sensor networks for long term monitoring of geological sequestration: Energy Conversion and Management, v. 47, p. 1968–1974, doi:10.1016/j.enconman.2005.09.010.

Schatzinger, R. A., 1988, Changes in facies and depositional environments along and across the trend of Horseshoe Atoll, Scurry and Kent Counties, Texas, *in* Cunningham B. K., editor, Permian and Pennsylvanian Stratigraphy Midland Basin, West Texas: Studies to Aid Hydrocarbon Exploration: Permian Basin Section, Society for Economic Paleontologists and Mineralogists Publication 88-28, p. 79–95.

Spycher, N., and Pruess, K., 2005, CO_2-H_2O mixtures in the geological sequestration of CO_2. II. Partitioning in chloride brines at 12–100°C and up to 600 bars: Geochimica et Cosmochimica Acta, v. 69, p. 3309–3320, doi:10.1016/j.gca.2005.01.015.

Spycher, N., and Pruess, K., and Ennis-King, J., 2003, CO_2-H_2O mixtures in the geological sequestration of CO_2. I. Assessment and calculation of mutual solubilities from 12 to 100°C and up to 600 bar: Geochimica et Cosmochimica Acta, v. 67, p. 3015–3031, doi:10.1016/S0016-7037(03)00273-4.

Stafford, P. T., 1957, Scurry field: Scurry, Kent and Border Counties, Texas, *in* Herald F. A., editor, Occurrence of Oil and Gas in West Texas: Bureau of Economic Geology, Austin, Texas, v. 5716, p. 295–302.

Steefel, C. I., and van Cappellen, P., 1990, A new kinetic approach to modeling water-rock interaction: The role of nucleation, precursors, and Ostwald ripening: Geochimica et Cosmochimica Acta, v. 54, p. 265–267, doi:10.1016/0016-7037(90)90003-4.

Stewart, R. W., ms, 1957, Reef limestones of the north Snyder oil field Scurry County, Texas: Department of Geology, Cambridge, Massachusetts, Massachusetts Institute of Technology, Cambridge, Ph.D. thesis.

Suekane, T., Nobuso, T., Hirai, S., and Kiyota, M., 2008, Geological storage of carbon dioxide by residual gas and solubility trapping: International Journal of Greenhouse Gas Control, v. 2, p. 58–64, doi:10.1016/S1750-5836(07)00096-5.

Svensson, U., and Dreybrodt, W., 1992, Dissolution kinetics of natural calcite minerals in CO_2-water systems approaching calcite equilibrium: Chemical Geology, v. 100, p. 129–145, doi:10.1016/0009-2541(92)90106-F.

Tester, J. W., Worley, W. G., Robinson, B. A., Grigsby, C. O., and Feerer, J. L., 1994, Correlating quartz dissolution kinetics in pure water from 25 to 625°C: Geochimica et Cosmochimica Acta, v. 58, p. 2407–2420, doi:10.1016/0016-7037(94)90020-5.

Thomas, D., and Benson, S., 2005, Carbon dioxide capture for storage in deep geologic formations: Results from the CO_2 capture project—Volume 2: Amsterdam, Elsevier, 1328 p.

Usdowski, E., 1994, Synthesis of dolomite and geochemical implications, *in* Purser, B., Tucker M., and Zenger D., editors, Dolomites: A volume in honor of Dolomieu: International Association of Sedimentologists, Special Publication n. 21: Oxford, Blackwell Scientific Publications, p. 345–360.

van der Meer, L. G. H., and van Wees, J. D., 2006, Limitations to storage pressure in finite saline aquifers and the effect of CO_2 solubility on storage pressure: San Antonio, Texas, USA, 24–27 September 2006, SPE Annual Technical Conference and Exhibition.

Vest, E. L., Jr., 1970, Oil Fields of Pennsylvanian—Permian Horseshoe Atoll, West Texas, *in* Halbouty, M. T., editor, Geology of Giant Petroleum Fields: AAPG Memoir 14, p. 185–203.

Walker, D. A., Golonka, J., and Reid, A. M., 1991, The effects of late Paleozoic paleolatitude and paleogeography on carbonate sediment in the Midland basin, Texas, *in* Candelaria M., editor, Permian Basin Plays, Tomorrow's Technology Today: West Texas Geological Society Publication 91-89, p. 141–162.

Watson, T. L., and Bachu, S., 2007, Evaluation of the potential for gas and CO_2 leakage along wellbores: E&P Environmental and Safety Conference, 5–7 March 2007, Galveston, Texas, SPE 106817.

Weeter, R. F., and Halstead, L. N., 1982, Production of CO_2 from a reservoir—A new concept: Journal of Petroleum Technology, v. 34, p. 2144–2148, doi:10.2118/10283-PA.

Wells, A. W., Diehl, J. R., Bromhal, G., Strazisar, B. R., Wilson, T. H., and White, C. M., 2007, The use of tracers to assess leakage from the sequestration of CO_2 in a depleted oil reservoir, New Mexico, USA: Applied Geochemistry, v. 22, p. 996–1016, doi:10.1016/j.apgeochem.2007.01.002.

White, S. P., 1995, Multiphase nonisothermal transport of systems of reacting chemicals: Water Resources Research, v. 31, p. 1761–1772, doi:10.1029/95WR00576.

White, S. P., Allis, R. G., Moore, J., Chidsey, T., Morgan, C., Gwynn, W., and Adams, M., 2005, Simulation of reactive transport of injected CO_2 on the Colorado Plateau, Utah, USA: Chemical Geology, v. 217, p. 387–405, doi:10.1016/j.chemgeo.2004.12.020.

Winthaegen, P., Arts, R., and Schroot, B., 2005, Monitoring subsurface CO_2 storage: Oil and Gas Science and Technology, v. 60, p. 573–582, doi:10.2516/ogst:2005040.

Wolery, T. J., and Daveler, S. A., 1992, EQ6, A computer program for reaction path modeling of aqueous

geochemical systems: Theoretical manual, user's guide and related documentation (version 7.0): Lawrence Livermore National Laboratory, Report UCRL-MA-110662 PT IV.

Wood, T. L., and Garrels, R. M., 1992, Calculated aqueous-solution-solid-solution reactions in the low-temperature system CaO-MgO-FeO-CO2-H2O: Geochimica et Cosmochimica Acta, v. 56, p. 3031–3043, doi:10.1016/0016-7037(92)90288-T.

Xu, T., Apps, J. A., and Pruess, K., 2004, Numerical simulation of CO_2 disposal by mineral trapping in deep aquifers: Applied Geochemistry, v. 19, p. 917–936, doi:10.1016/j.apgeochem.2003.11.003.

——— 2005, Mineral sequestration of carbon dioxide in a sandstone-shale system: Chemical Geology, v. 217, p. 295–318, doi:10.1016/j.chemgeo.2004.12.015.

Xu, T., Sonnenthal, E., Spycher, N., and Pruess, K., 2006, TOUGHREACT—A simulation program for non-isothermal multiphase reactive geochemical transport in variably saturated geologic media: Applications to geothermal injectivity and CO_2 geologic sequestration: Computers and Geoscience, v. 32, p. 145–165, doi:10.1016/j.cageo.2005.06.014.

Yamamoto, H., and Doughty, C., 2009, Investigation of gridding effects for numerical simulation of CO_2 geologic sequestration: Berkeley, California, Lawrence Berkeley National Laboratory, September 14–16, 2009, Proceedings of TOUGH Symposium.

Zerai, B., Saylor, B. Z., and Matisoff, G., 2006, Computer simulation of CO_2 trapped through mineral precipitation in the Rose Run Sandstone, Ohio: Applied Geochemistry, v. 21, p. 223–240, doi:10.1016/j.apgeochem.2005.11.002.

Zhang, G., Spycher, N., Sonnenthal, E., and Steefel C., 2006, Implementation of a Pitzer activity model into TOUGHREACT for modeling concentrated solutions: Berkeley, California, Lawrence Berkeley National Laboratory, May 15–17, 2006, Proceedings of TOUGH Symposium.

Zhang, W., Li, Y., Xu, T., Cheng, H., Zheng, Y., and Xiong, P., 2009, Long-term variations of CO_2 trapped in different mechanisms in deep saline formations: A case study of the Songliao Basin, China: International Journal of Greenhouse Gas Control, v. 3, p. 161–180, doi:10.1016/j.ijggc.2008.07.007.

Zhou, Q., Birkholzer, J. T., Tsang, C.-F., and Rutqvist, J., 2008, A method for quick assessment of CO_2 storage capacity in closed and semi-closed saline formation: International Journal of Greenhouse Gas Control, v. 2, p. 626–639, doi:10.1016/j.ijggc.2008.02.004.